UHASSELT
KNOWLEDGE IN ACTION

Maastricht University

# Faculty of Medicine and Life Sciences
## *School for Life Sciences*
## Master of Biomedical Sciences

***Masterthesis***

***Leukocyte- and Platelet Rich Fibrin, an autologous biomaterial to improve regeneration of large gap peripheral nerve injuries***

**Lien Coekaerts**

Thesis presented in fulfillment of the requirements for the degree of Master of Biomedical Sciences, specialization Clinical Molecular Sciences

**SUPERVISOR :**

Prof. dr. Ivo LAMBRICHTS

**MENTOR :**

De heer Tim VANGANSEWINKEL

2017
2018

Transnational University Limburg is a unique collaboration of two universities in two countries: the University of Hasselt and Maastricht University.

UHASSELT
KNOWLEDGE IN ACTION

**www.uhasselt.be**
Universiteit Hasselt
Campus Hasselt:
Martelarenlaan 42 | 3500 Hasselt
Campus Diepenbeek:
Agoralaan Gebouw D | 3590 Diepenbeek

UHASSELT
KNOWLEDGE IN ACTION

Maastricht University

# Faculty of Medicine and Life Sciences
## *School for Life Sciences*
## Master of Biomedical Sciences

***Masterthesis***

***Leukocyte- and Platelet Rich Fibrin, an autologous biomaterial to improve regeneration of large gap peripheral nerve injuries***

**Lien Coekaerts**

Thesis presented in fulfillment of the requirements for the degree of Master of Biomedical Sciences, specialization Clinical Molecular Sciences

**SUPERVISOR :**

Prof. dr. Ivo LAMBRICHTS

**MENTOR :**

De heer Tim VANGANSEWINKEL

## Acknowledgements

Ever since I was little I have been very interested in finding out how things work. I'm sure my parents can testify that they had to answer a lot of questions starting with 'How…?' and 'Why …?', until they finally gave me a book called "the how and why of everything" which sparked my interest in science. As I got older I remained curious, and this lead to my decision to start my studies in biotechnology. Which later evolved to my decision to start my studies in the very interesting field of biomedical sciences.

I am grateful to prof. dr. Ivo Lambrichts for giving me the opportunity to work in his research group on the topic of peripheral nerve injuries, which I really enjoyed immersing myself in during the last eight months. Hereby, I would also like to thank the whole morphology group for creating an enjoyable work atmosphere.

I really want to thank my daily supervisor Tim Vangansewinkel. From the start of the internship he was always ready to answer any of my many questions. We had many interesting and insightful talks that helped me understand peripheral nerve injury and L-PRF better. He always explained things to me very well and thereby helped me to fully understand everything. Furthermore, he taught me a lot of new techniques in the lab, and was always ready to assist me when necessary. He frequently checked if everything was still going OK and if I needed anything. Additionally, I would also like to thank him for his many helpful corrections during the writing of my thesis. Lastly, I want to thank him for donating his time to give me this amazing internship. I enjoyed myself so much that it hardly even seems that eight months have passed since I started.

Next, I would also like to thank my second supervisor dr.Tim Vanmierlo for his many interesting remarks during the progress meeting. I also want to thank him for his excellent suggestions to help me strengthen my study. Furthermore, I would like to thank dr.Nick Smisdom for the many hours he helped us with making excellent confocal images seen in my thesis. His help in figuring out how to get these excellent images from the complicated software to a thesis-worthy picture was also much appreciated. I am also very grateful, that he made time to help me with writing and correcting my confocal microscopy methods part of my thesis. Next, I would also like to thank Leen Timmermans for generously lending me her computer so that I could have access to the NEO-software, after the very unfortunate crash of the only other computer that contained this software. Without her I would not have been able to analyse some very important data necessary to make a good conclusion in the *in vitro* part of my thesis. Also, I would like to thank the people a IMO, without whose excellent help I would not have been able to obtain the beautiful SEM-images seen in my thesis.

Lastly, I would also like to thank all my classmate for the many laughs and distracting conversations and without who the year would have been much less fun. I also want to thank my parents and siblings for supporting me during my studies.

## Table of contents

## List of abbreviations

| | |
|---|---|
| **bFGF** | Basic fibroblast growth factor |
| **BDNF** | Brain-derived neurotrophic factor |
| **CAM** | Cell adhesion molecules |
| **CNS** | Central nervous system |
| **CM** | Conditioned medium |
| **DAM** | Donkey anti-mouse |
| **DAPI** | 4',6-diamidino-2-phenylindole |
| **DARb** | Donkey anti-rabbit |
| **DMEM** | Dulbecco's Modified Eagle's Medium |
| **DNase** I | Deoxyribonuclease I |
| **DRG** | Dorsal root ganglion |
| **ECM** | Extracellular matrix |
| **ELISA** | Enzyme-linked immunosorbent assay |
| **FCS** | Foetal calf serum |
| **GAM** | Goat anti-mouse |
| **GARb** | Goat anti-rabbit |
| **GDNF** | Glial-derived neurotrophic factor |
| **GF** | Growth factor |
| **GFAP** | Glial fibrillary acidic protein |
| **HLA-DR** | Human Leukocyte Antigen – antigen D Related |
| **IGF-1** | Insulin-like growth factor-1 |
| **L-PRF** | Leukocyte- and Platelet-Rich Fibrin |
| **MAG** | Myelin-associated glycoprotein |
| **MBP** | Myelin basic protein |
| **NCAM** | Neural cell adhesion molecules |
| **NGF** | Nerve growth factor |
| **NT-3** | Neurothropin-3 |
| **O/N** | Overnight |
| **PBS** | Phosphate buffered saline |
| **PDGF-BB** | Platelet-derived growth factor-BB |
| **PDL** | Poly-D-lysine |
| **PFA** | Paraformaldehyde |
| **PNI** | Peripheral nerve injury |
| **PNS** | Peripheral nervous system |
| **PPP** | platelet poor plasma |
| **PRF** | Platelet Rich Fibrin |
| **PRP** | Platelet Rich Plasma |
| **P/S** | Penicillin/streptomycin |
| **RI** | Regularity index |
| **rpm** | Rotations per minute |
| **RT** | Room temperature |
| **TEM** | Transmission electron microscopy |
| **TGF- β1** | Transforming growth factor β1 |
| **SC** | Schwann cell |
| **SEM** | Scanning electron microscopy |
| **SEM** | Standard error of the mean |
| **SFI** | Sciatic function index |
| **VEGF-A** | Vascular endothelial growth factor-A |

## Abstract

**Introduction.** Peripheral nerve injuries (PNI) represent a major clinical concern worldwide. Especially large gap PNIs are problematic as current treatment options (e.g. autografts, nerve conduits) are insufficient to completely restore lost functions. In our study we focus on a new therapeutic approach by employing a platelet concentrate to augment peripheral nerve regeneration after injury. Leukocyte- and Platelet-Rich Fibrin (L-PRF) is a second-generation platelet concentrate consisting of a fibrin network that contains growth factors (GFs), platelets and leukocytes. We hypothesise that L-PRF promotes functional recovery after large gap nerve injuries by stimulating and supporting axon regeneration.

**Materials and methods.** As a first step, we characterized the morphology of L-PRF by using several histological techniques such as Masson's trichome staining, confocal microscopy, transmission electron microscopy and scanning electron microscopy. Secretome analysis was performed to analyse the GFs released by L-PRF, this by an antibody array and enzyme-linked immunosorbent assay (ELISA) on L-PRF exudate and conditioned medium (CM). Next, we determined the effect of L-PRF on neurite outgrowth and survival by stimulating dorsal root ganglion (DRG) neurons with different concentrations of exudate and CM. Finally, a pilot experiment was performed *in vivo* to test the neuroregenerative capabilities of L-PRF in a rat model for PNI.

**Results.** Morphological analysis showed that L-PRF consists of two definable areas: the fibrin matrix, and the cell-rich area separated by a platelet-rich zone. The largest part of the L-PRF clot consists of a dense network of fibrin fibres, and clusters of blood platelets are distributed throughout this matrix. The cell-rich area is located on one side of the clot, and contains mainly leukocytes (e.g. neutrophils, monocytes). Secretome analysis showed that a plethora of GFs are present in L-PRF exudate and CM, such as BDNF, GDNF, NT-3, NGF, PDGF and VEGF. More importantly, we observed that these factors are slowly released over time from the fibrin clot. In addition, we found a positive dose-dependent effect of L-PRF CM on neurite growth and survival of DRG neurons in culture. Finally, our *in vivo* pilot experiment showed that decellularized blood vessels are suitable to implant L-PRF between nerve endings. Moreover, we observed a decline in the functional outcome two weeks post injury in all groups. We also observed an increased cell infiltration into the regenerating nerves two-weeks post-surgery.

**Conclusion.** L-PRF is an autologous biomaterial that has several advantages in terms of biocompatibility and safety. It can be easily obtained from the patient's own blood which makes it ideal for clinical applications. In our study, we demonstrated that L-PRF consists out of a fibrin matrix that can support regenerating axons. Furthermore, we confirmed that L-PRF slowly releases many growth factors that positively affect neuronal cell survival, and neurite growth *in vitro*. The pilot study showed that L-PRF supports axon regeneration, and aids cell infiltration the first weeks after injury. In conclusion, our data provides good evidence that L-PRF can be used as an alternative therapy to repair large gap nerve defects. However, further characterization of this biomaterial both *in vitro* and *in vivo* is necessary to understand its full potential as a therapy for peripheral nerve repair.

## Samenvatting

**Introductie.** Perifere zenuwschade is een van de grote klinische problemen in de wereld. Met de huidige behandelingen (bv. autoloog zenuwtransplantaat, zenuw conduit) is het moeilijk om een volledig functieherstel te krijgen. Daarom focussen wij ons op bloedplaatjes concentraten die mogelijks het zenuwherstel na schade kunnen bevorderen. Leukocyt- en plaatjes-rijk fibrine (L-PRF) is een 2$^{e}$ generatie bloedplaatjes concentraat dat bestaat uit een fibrine netwerk waarin groeifactoren (GF), bloedplaatjes en leukocyten zitten. Onze hypothese is dat L-PRF het functioneel herstel na zware zenuwschade kan bevorderen door de zenuwgroei te stimuleren en te ondersteunen.

**Materiaal en methoden.** Als eerste stap hebben we de morfologie van L-PRF gekarakteriseerd door verscheidende histologische technieken toe te passen zoals een Masson's trichome kleuring, confocale microscopie, transmissie elektronenmicroscopie en scanning elektronenmicroscopie. Vervolgens hebben we een secretoom analyse op L-PRF gedaan om de vrijgelaten GF te analyseren in het exsudaat en geconditioneerd medium (CM) van L-PRF. De secretoom analyse werd uitgevoerd doormiddel van een antibody array en een enzyme-linked immunosorbent assay (ELISA). Hierna hebben we het effect van L-PRF op de neuriet uitgroei en cel overleving getest door dorsal root ganglion (DRG) neuronen te stimuleren met verschillende concentraties van het L-PRF exsudaat en CM. Als laatste hebben we een *in vivo* piloot experiment uitgevoerd om de neuroregeneratieve effecten van L-PRF te testen in een rat model voor zenuwschade.

**Resultaten.** Uit de morfologische analyse bleek dat L-PRF uit twee definieerbare gebieden bestaat: de fibrine matrix en het cel-rijke gebied die gescheiden zijn door een zone rijk aan bloedplaatjes. Het grootste deel van het L-PRF bestaat uit een netwerk van fibrinevezels met clusters van bloedplaatjes die verdeeld zijn in deze matrix. Het cel-rijke gebied bevindt zich aan één kant van L-PRF en bevat voornamelijk leukocyten (bv neutrofielen, monocyten). Uit de secretoom-analyse bleek dat er veel verschilleden GF in het exsudaat en CM van L-PRF zitten, namelijk BDNF, GDNF, NT-3, NGF, PDGF en VEGF. Deze GF worden bovendien ook traag vrijgegeven door de fibrine matrix in verloop van tijd. We zagen ook dat het L-PRF CM een positief dosisafhankelijk effect heeft op neurietgroei en de overleving van DRG-neuronen in kweek. Uit ons *in vivo* piloot experiment bleek dat de gedecellulariseerde bloedvaten geschikt zijn voor de implantatie van L-PRF tussen twee zenuwuiteinden. We zagen ook nog dat 2 weken na de verwonding er nog geen functioneel herstel had opgetreden maar er was wel al een verhoogde cel infiltratie in de regenererende zenuw na twee weken.

**Conclusie.** L-PRF is een autoloog biomateriaal dat verschillende voordelen heeft op het gebied van bio-compatibiliteit en veiligheid. L-PRF is ideaal voor klinische toepassingen omdat het makkelijk verkregen kan worden van het eigen bloed van de patiënt. In onze studie hebben we aangetoond dat L-PRF verschillende GF traag over verloop van tijd uitscheidt en dat deze GF positief zijn voor de neuronale overleving en zenuwgroei *in vitro*. De piloot studie heeft ook aangetoond dat L-PRF de zenuwgroei ondersteund en in de eerste weken van het herstel de cel infiltratie bevordert. We kunnen uit onze data concluderen dat L-PRF mogelijks gebruikt kan worden als een alternatieve therapie voor het herstel van zware zenuwschade. Maar om zekerheid te hebben moet L-PRF nog meer gekarakteriseerd worden en dit zowel *in vitro* als *in vivo* zodat we het volledige potentieel van L-PRF kunnen onderscheiden.

# 1. Introduction

## 1.1 Peripheral nerve injury

The peripheral nervous system (PNS) is the nervous system outside of the brain and spinal cord that is responsible for conducting signals that originate from the spinal cord to the rest of the body. The nerves in the PNS are a combination of sensory, motor, and autonomic nerves. Furthermore, the PNS contains three cell types, namely the neurons, glial cells and stromal cells. The stromal cells form the connective tissue surrounding the nerves. However, the Schwann cells (SC) play an important role in the maintenance and function of the peripheral nerves. SCs myelinate the nerves which aids the conduction velocity. They also produce several neurotropic factors to support the nerves (1, 2).

A peripheral nerve injury (PNI) is a common injury; it is estimated that in developed countries between 13 to 23 persons per 100,000 are injured (3). PNI's are most often caused by traumatic insults, but also some medical disorders, such as Guillain-Barre syndrome and Charcot Marie Tooth disease, that can affect the function of the peripheral nervous system (PNS). Traumatic nerve injury can be induced for example by mechanical, thermal, chemical or ischemic insults (2, 3). The largest consequence of these injuries is the loss of communication through sensory and/or motor nerves between the central nervous system (CNS) and the peripheral organs (e.g. skeletal muscle, nerve endings in the skin). As a direct effect of their injuries, patients with PNI may experience a substantial decrease in quality of life, and it also has a significant socio-economic impact. These patients need to learn how to live with a partial or full paralysis. However, in contrast to the CNS, the PNS has the potential to repair itself after injury but this depends on several conditions such as the severity of the lesion. Peripheral axons can regenerate after injury; in general, they can grow around 1 mm/day, and they may eventually re-establish a connection with their target organ (2-4). However, it is a very slow healing process that can even take up 12 to 18 months before functional recovery is established. It is important to keep in mind that re-innervation does not automatically mean there is complete functional recovery. Many PNIs never heal properly as the endogenous repair response is often incomplete, meaning that there is a great need for a therapy that can speed up repair processes after injury. An example of problematic nerve injuries are the large gap nerve defects, in these injuries the nerve gap exceeds more than two cm. The regeneration of these large defects is difficult because of the distance the nerves have to bridge in order to reform a connection with their target (e.g. skeletal muscle) (1-5).

### 1.1.1 Pathophysiology PNI

Several degenerative processes are initiated when a peripheral nerve gets injured. The distal nerve ending gets disconnected from the body, and it will degenerate via a process that is called Wallerian degeneration (Figure 1). The axon is fragmented by proteases and all components of the nerve are disintegrated in the first 24 to 36h after injury. The myelin sheath is also degraded (2, 4, 6). Macrophages will start to infiltrate the injury site and they help to clear axonal and myelin-derived debris. Within 24h after the injury, SCs will start to proliferate and switch their phenotype from a myelinating to a more regenerative profile. The denervated SCs will down-regulate several structural

proteins such as myelin basic protein (MBP) and myelin-associated glycoprotein (MAG) whilst up-regulating cell adhesion molecules (CAM) and several growth factors. These up-regulated CAM are L1, neural CAM (NCAM), and glial fibrillary acidic protein (GFAP). The most important growth factors produced by SCs after nerve injury are nerve growth factor (NGF), brain-derived neurotrophic factor (BDNF), glial-derived neurotrophic factor (GDNF), basic fibroblast growth factor (bFGF) and neurotrophin 3 (NT-3). It is well known that these growth factors play a role in stimulating the nerve regeneration (4). At the proximal end, several cellular and molecular changes take place in the damaged neural cell body after injury. The nerve starts to swell but there is minimal degeneration. The SC and macrophages in the injury site will also produce interleukin-6 to stimulate more SC and fibroblast proliferation (6). When all the debris is removed the regeneration starts at the proximal nerve ending. New axonal sprouts develop and start to grow from the Ranvier nodes located closest to the proximal nerve ending. SCs will begin to proliferate and align themselves between basal membranes of the two nerve ends and form the so-called bands of Büngner at the distal end which will serve to guide the axonal sprouts. The axonal growth cone will also release several proteases to aid regeneration through tissue (2, 4). Multiple axonal extensions will grow from the growth cone in an attempt to contact the target at the distal end of the nerve injury. Axonal sprouts that do not reach the target are checked by the 'pruning' of the growth cones, however, if the sprouts are not degenerated a neuroma may form because of misdirection. The new axonal sprouts become myelinated and they can reconnect with their original target (e.g. skeletal muscle), possibly resulting in recovery of functions that were lost due to initial traumatic insult. As mentioned before, axons that sprout form the proximal end will grow about 1 mm each day. In case axonal sprouts are not able to reconnect with their target it is possible that because of lack of neuronal contact to the distal end the SCs will down regulate their growth factors, and switch to a dormant phenotype, halting all axonal growth (2, 4, 6).

Nerve injuries can be subcategorized according to Seddon or Sunderland's classification. Seddon's classification of nerve injury can be divided in neuropraxia, axonotmesis, and neurotmesis. The least severe type of PNI, neuropraxia (Sunderland's 1st degree injury), still has intact axons and no Wallerian degeneration will take place. Although there is partial demyelination meaning that some impulses cannot be transmitted efficiently anymore. When the cause of the injury is removed, neuropraxia usually heals fully without any problems. Second, there is axonotmesis, this Seddon classification encompasses the 2$^{nd}$, 3$^{rd}$ and 4$^{th}$ Sunderland classifications. In Sunderland's 2$^{nd}$ degree injury the axon is severed but the endoneurium remains intact. In the 3$^{rd}$ degree classification the endoneurium is disrupted but the fascicular arrangement and perineurium remains preserved. When this is the case the functional recovery can be delayed because fibrosis can take place within the fascicles. Lastly, in the 4$^{th}$ degree injury only the epineurium is still intact while the disruption occurs in the axons, endoneurium and perineurium. During axonotmesis, Wallerian degeneration takes place distally, degenerating the myelin, and axons that are present there. However, part of the original nerve supporting structure still remains intact and has the potential to guide new axonal sprouts (2, 6). The most severe type of nerve injury is neurotmesis which corresponds with Sunderland's 5$^{th}$ degree injury. This is the category that large gap PNIs fall in, these injuries always require surgical repair. Neurotmesis is defined by a complete transection of the nerve and thus total loss of function

below the injury. Here, there is also Wallerian degeneration of the distal ends and possible neuroma formation at the proximal end when no intervention takes place (2, 6).

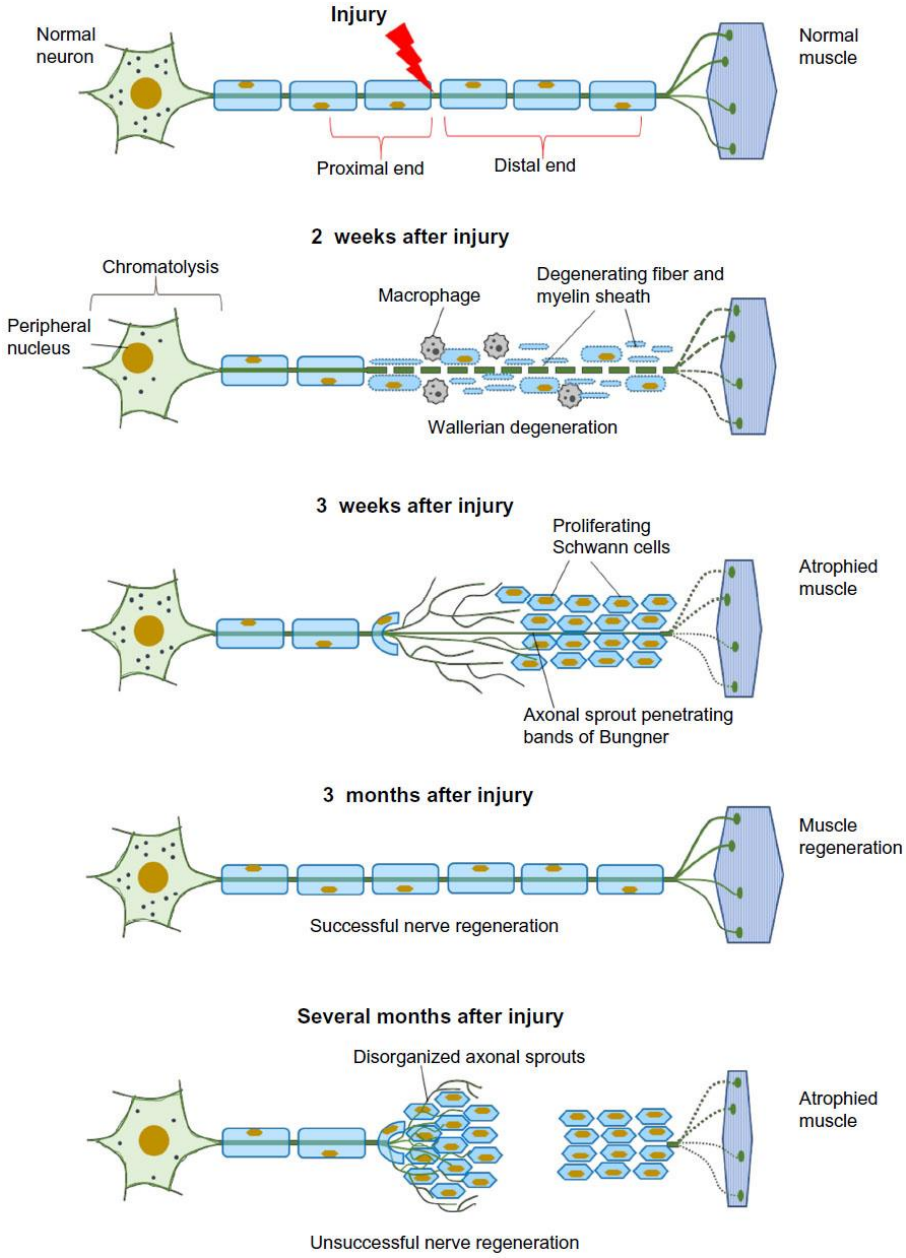


**Figure 1: Overview of the pathophysiological processes after peripheral nerve injury.** After nerve injury, Wallerian degeneration takes place, the distal nerve end is degenerated during this process. Macrophages infiltrate and help clear axonal and myelin-derived debris. Also at the proximal end, several changes take place, such as swelling of the cell body (chromatolysis). When the debris is cleared, axonal sprouts will grow from the proximal end. Schwann cells proliferate and form bands of Büngner that support regenerating axons. After a few months the repair process is complete when regenerating axons reconnect to their target organ (e.g. skeletal muscle). Alternatively, it is possible that the regenerative process fails and that neuroma formation occurs. Image obtained from Arslantunali et. al (2).

### 1.1.2 Therapy for Peripheral Nerve Injury

Currently, there are only a few therapies available for PNIs, especially large gap PNIs present a big challenge. For shorter gaps (< 5 mm) where the two nerve ends can be realigned without creating tension, simple epineural microsutures can be used to repair the nerve. However, this method cannot be employed for large gap injuries as the distance between the nerve ends is too big to reconnect them. Suturing of big gaps will create too much tension on the nerves which is detrimental for the regeneration (3, 5, 7, 8). For large gap nerve injuries alternative therapies are used in the clinic. Autografts (i.e. autologous nerve graft) are currently the "gold standard" therapy, and give the best results in repairing large gap nerve injuries. The big advantage of autografts is that a nerve is taken from the patient themselves. Therefore, it elicits no immune reaction, and it mimics the native environment as it keeps its supporting matrix and contains SCs.(3). However, the end results with autografts are not always optimal and they have also several disadvantages. A healthy functioning, but less important nerve is sacrificed to create the autograft, and extensive surgery is required as the patient is operated on in two different places. Furthermore, autografts are limited by the amount of healthy nerve available, and a morphometric mismatch often occurs which is adverse for regeneration. Morphometric mismatches are created because not every nerve is the same size, and also the fascicles can be organised in different ways. In the clinic, most often sensory nerves are used as autografts to repair defects in motor nerves for example (4, 5, 7, 8). When autografts are not available, allografts are frequently used, here the donor nerve for the graft comes from a cadaver or another person. This type of nerve graft can provide guidance and viable SCs to help stimulate axon regeneration. However, the downside of allografts is that patients must take immunosuppressants which can lead to opportunistic infections and sometimes even tumour formation (3).

In the last decade, various nerve conduits have been designed as an alternative therapy for the autograft treatment. Nerve conduits increase the functional repair in gaps shorter than three cm, placing conduits in larger gaps would be adverse for the regeneration. This limitation occurs because SCs do not migrate more than two cm into the conduit meaning that after two cm axon outgrowth is hampered (3, 5). The conduit works as a tube to guide the axonal regeneration of the nerve from the proximal to the distal end. Despite guidance, the conduit itself has no impact on the regeneration process. Thus, sometimes conduits are enhanced by adding lumen-fillers such as growth factors, cells (e.g. Schwann cell differentiated dental pulp stem cells), matrix proteins (e.g. collagen, laminin, hydrogels), and filaments (e.g. synthetic, collagen). Conduits have several advantages over autografts. There is no need to harvest a nerve, no differences in host-donor nerve diameters, no mismatches in number or organisation of fascicles, and no morbidity of the donor area takes place (3, 5, 9, 10). There are several specifications a good conduit should have. Firstly, a conduit should follow the orientation of the nerve pathway. Furthermore, a conduit should be flexible, and not easily collapsible. The conduit should be permeable, to allow for fluid and cellular exchange, and diffusion of oxygen between the regenerating tissue and the tissue around the conduit. Recently, more focus is also put on the biodegradability of conduits. Currently, most conduits are made out of different biomaterials of which only some are biodegradable (3, 11). Several natural materials are used

frequently as conduits. These materials include skeletal muscles, tendons, and blood vessels. The most popular of these are the vein conduits. Natural materials are much more biocompatible than synthetic materials. Furthermore, the use of natural materials gives less toxicity, and can enhance the migration of support cells into the injured area. Non-degradable synthetic materials, such as silicone, elastomer hydrogel and porous stainless steel, have also been used as conduits. Although, the synthetic conduits can guide the regeneration, they are still recognised as a foreign body by the immune system. Synthetic materials can lead to inflammation which in turn can then lead to scar formation. Therefore, the use of biodegradable materials, such as collagen, polyglycolic acid, chitosan, polyesters, and polylactic acid are more interesting to use as conduits. These conduits are slowly degraded after the nerve regeneration has taken place. Because the conduits are degraded only a mild foreign antibody reaction is present (3, 5, 11).

Despite these different options to treat PNI, there is still no perfect solution. A lot of patients that have undergone surgical intervention never heal properly. The nerve damage incurred will be present for life, along with the disabilities associated with the injury. One meta-analysis encompassing more than 600 patients with median or ulnar nerve injuries has even shown that after surgical treatment only 51,6% of patients will achieve an acceptable motor recovery, while for sensory recovery only 42,6% is satisfied (12). Despite the massive increase in knowledge in the field of neuroscience over the last decades, the treatments for PNIs haven't changed or improved. The nerve pathophysiology is much better understood but surgeons still use autografts and nerve conduits, both first described decades ago (5, 13, 14). This all signifies the need for the development of an improved treatment that can better establish functional repair of the nerve in large gap injuries (5, 7, 8).

## 1.2 Leukocyte - and Platelet-Rich Fibrin

Different biomaterials and pharmaceutical preparations have been developed to improve wound healing. Hereby, researchers attempt to mimic and/or enhance the natural processes that occur during wound healing, such as the haemostasis. After injury, the coagulation cascade ensures that the blood vessels are sealed off again with platelets which become activated and aggregate. Platelets are not only important to seal the injury, but they also excrete a lot of fibrinogen, growth factors and enzymes necessary for the healing process. The coagulation cascade includes the fast formation of a new temporary solid tissue that is composed of a dense fibrin matrix interspersed with platelets and leukocytes. This formed matrix attracts more platelets, leukocytes, and allows for the migration and differentiation of different surrounding cells to the fibrin network, thereby, the matrix helps to guide the healing. As the matrix is remodelled and transformed at a later stage, it serves as an excellent basis for the tissue regeneration. This natural process is the foundation for the development of platelet concentrates as tools in regenerative medicine (15-17).

The first platelet concentrate that was developed is the Platelet Rich Plasma (PRP) concentrates. Many different protocols exist for the creation of platelet concentrates all based on the same principle. Blood is collected from the patient, and then centrifuged to separate the components resulting in PRP, a liquid mixture with a high concentration of platelets and rich in growth factors. PRP is produced

with the presence of anticoagulants. Often PRP are centrifuged twice to increase their platelet concentration even more. In the clinic, PRP is frequently applied for the prevention and treatment of haemorrhages (15, 16). Later, second-generation platelet concentrates were developed by Choukroun *et al*., and given the name Platelet-Rich Fibrin (PRF) (18). PRF has a slightly different production process than PRP as it is centrifuged without the addition of anticoagulants. The biggest difference between PRP and PRF is the fibrin concentration which is much higher in PRF. PRF concentrates thus form a fibrin clot filled with serum and activated platelets. During the production of PRF, the platelets present in the blood are activated and trapped in the fibrin matrix. The activated platelets release several growth factors and cytokines which are subsequently also trapped in the fibrin matrix, and slowly released over time (15, 16, 19-21). Platelet concentrates are currently implemented in clinical settings as surgical adjuvants in different surgical disciplines. These disciplines include oral and maxillofacial surgery, Ear-Nose-Throat surgery, plastic surgery, orthopaedics and trauma surgery, sports medicine, general surgery, gynaecologic and cardiovascular surgery (15). Platelet concentrates can be applied to aid the healing process in therapies with tissues that lack a sufficient blood supply, have a slow cell turnover, and possess only limited extracellular matrix (ECM) repair (19).

Leukocyte- and Platelet Rich Fibrin (L-PRF) is a subdivision of the second-generation platelet concentrates. As the name L-PRF states the difference between PRF and L-PRF is the presence of leukocytes. L-PRF, like all platelet concentrates, is an autologous biomaterial that is easily obtained from the peripheral blood. As it is classified as a PRF, it has a high fibrin concentration that is arranged in a dense matrix. Furthermore, L-PRF contains a high concentration of growth factors, platelets, and leukocytes. Therefore, L-PRF provides all the molecular and cellular elements needed to promote healing (19-22).The growth factors present in L-PRF are trapped in the fibrin matrix, and released slowly over a period of several days (19-21). Several studies have shown that growth factors secreted by L-PRF are still detectable after more than seven days. These studies have also shown that the growth factors secreted by L-PRF include transforming growth factor β1 (TGF-β1), platelet-derived growth factor (PDGF), insulin-like growth factor-1 (IGF-1), and vascular endothelial growth factor (VEGF). Furthermore, matrix proteins such as fibronectin, vitronectin and thrombospondin-1 have also been detected in L-PRF secretions. All these growth factors are beneficial for angiogenesis, cell proliferation, and matrix remodelling. In other words, these growth factors stimulate healing of the tissue (15, 17, 19).

## 1.3 Objectives and experimental design

In this study, we aim to elucidate the neuroregenerative potential of L-PRF by using several *in vitro* assays and an *in vivo* model for PNI. L-PRF has several advantages, like the potential to induce regenerative processes by releasing growth factors, and provide structural support for regenerating axons with its fibrin matrix. Therefore, we propose that L-PRF is a suitable biomaterial that can be used for tissue engineering of an injured nerve. We hypothesized that L-PRF promotes functional recovery after large gap nerve injuries by stimulating and supporting the axon regeneration.

Stimulating by the slow release of growth factors from the L-PRF fibrin matrix. These growth factors can support the wound healing, and axon regeneration. Furthermore, the L-PRF fibrin matrix can support the axon regeneration. The matrix can serve as a preliminary guide for the regeneration. Our hope is that in the future, our findings can lead to the development of a novel and more effective treatment for PNI, and therefore improve the quality of patients' lives.

As we want to use L-PRF for tissue engineering purposes, our first step is to characterize the morphology, and 3D-fibrin structure. The structure of L-PRF will be identified by histological staining. Furthermore, we will analyse the ultrastructure of L-PRF by scanning electron microscopy (SEM), and transmission electron microscopy (TEM) to determine the distribution of both platelets and leukocytes in the L-PRF fibrin matrix. Additionally, the porosity, and the presence of other matrix components in L-PRF will be analysed by confocal microscopy.

We will examine the secretome of L-PRF by first performing a screening for many different proteins that are released from L-PRF with an antibody array. We want to identify the growth factors present in the L-PRF exudate, and the L-PRF conditioned medium (CM). Exudate is the fluid collected after compressing the L-PRF clot and CM is the culture medium in which a L-PRF clot was immersed. Afterwards, we will analyse the release pattern, and the exact concentration of several growth factors by enzyme-linked immunosorbent assay (ELISA). For the ELISA we will focus on growth factors that are known to have a positive effect on nerve regeneration. The intention of this secretome analysis is to show that L-PRF is a great reservoir of growth factors, and that these growth factors are released slowly over time.

As a next step, we will determine if the growth factors of L-PRF influence the cell survival, and neurite outgrowth of dorsal root ganglion (DRG) neurons *in vitro*. Therefore, we will culture DRGs under serum deprived conditions, and stimulate them with L-PRF exudate and CM. After stimulation, we will quantify the presence of DRG neurons and their neurites in the culture.

Finally, we will investigate the neuroregenerative capabilities of L-PRF *in vivo* in a rat model for PNI. A 5 mm gap nerve defect will be induced in the left sciatic nerve in rats, and this gap will be reconnected by the use of the fibrin- and platelet-rich area of an L-PRF clot. To implant L-PRF between nerve endings we aim to use a decellularized blood vessel, but first we must explore the use of this conduit in more detail in this study as well. We will also include an autograft group (i.e. gold standard treatment in the clinic), and a group that receives an empty blood vessel conduit. Functional recovery of the rats will be followed by walking track analysis to assess changes in the gait. Afterwards, we will use immunostaining and several other histological techniques to assess the regeneration of the axons, and the initial cell infiltration into the regenerating nerve.

# 2. Materials and Methods

## 2.1 Sample preparation of Leukocyte- and Platelet- Rich Fibrin

Blood samples were obtained from healthy donors with informed written consent. This study protocol and consent procedure were approved by the medical ethical committee from Hasselt University and the Clinical Trial Center from KU Leuven (S58789/B322201628215). All experiments were performed in accordance to the relevant guidelines and regulations. Blood samples were collected in glass-coated plastic tubes (VACUETTE® 9 mL Z Serum Clot Activator Tubes, Greiner Bio-One, Kremsmünster, Oostenrijk) via venipuncture, and these tubes were immediately centrifuged (IntraSpin™ Centrifuge, Intra-Lock, Boca Raton, Florida, USA) for 12 minutes (min) at 2700 rotations per minute (rpm) (400 g). During centrifugation the blood coagulates, and forms the L-PRF clot which is located in between the red blood cells, and the platelet poor plasma (PPP) in the middle of the plastic tube.

For the preparation of conditioned medium (CM) (Figure 2), L-PRF clots were incubated in 6 well plates (Greiner Bio-one) with 6 mL Dulbecco's Modified Eagle's Medium (DMEM, D5796 Sigma-Aldrich, Overijse, Belgium) supplemented with 100 U/mL Penicillin and 100 µg/mL Streptomycin (1% P/S, Sigma-Aldrich). These L-PRF clots were cultured at 37°C in a humidified atmosphere with 5% $CO_2$. Conditioned medium (CM) was collected, and replaced by fresh medium, at 24h, 48h, 96h, and 144h to analyse the release of growth factors in time. A L-PRF clot was discarded, when the clot dissolved before all CM conditions were collected. The collected medium was centrifuged for 6 min at 300 g, sterile filtered (0.2 µm, VWR, Leuven, Belgium) and stored at -80°C until further usage. In addition, this same CM collection process was used to collect the cumulative CM after 96h ("total CM"). To collect exudate, fresh L-PRF clots were transferred to a sterile box (Xpression™ Fabrication Box, Intra-Lock) and pressed into thin membranes, thereby releasing exudate, which was filtered and stored at -80°C as described.

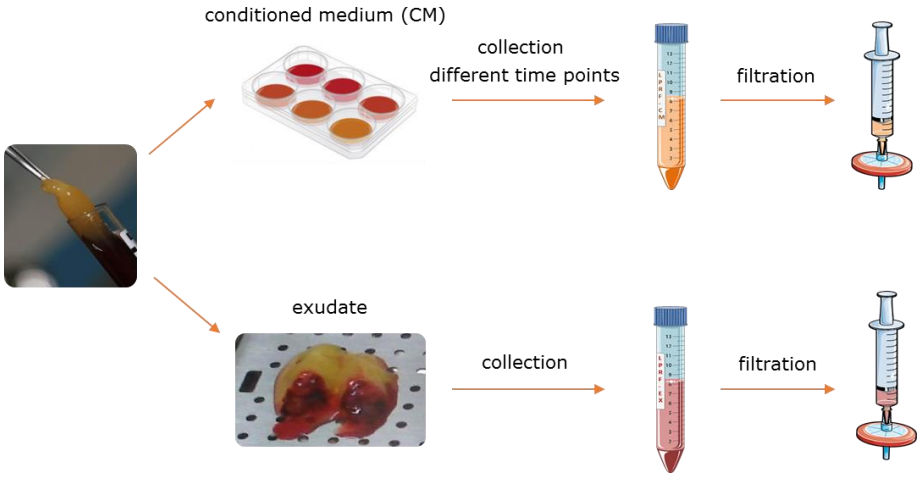


**Figure 2: Schematic view of the conditioned medium and exudate preparation.** L-PRF was placed in a 6-well plate and 6ml Dulbecco's Modified Eagle's Medium (DMEM, D5796) was added. The conditioned medium (CM) was collected at 24h, 48h, 96h, and 144h, and then centrifuged (6 min 300g). Lastly, the CM was filtered (0.2 µm). Exudate was made by pressing clots into thin membranes. All released fluid, the exudate was collected, and then filtered (0.2 µm)

## 2.2 Morphological characterization of Leukocyte-and Platelet-Rich Fibrin

### 2.2.1 Masson's trichome staining

A Masson's trichome staining was done on L-PRF paraffin sections of 8 µm thickness. The sections were first deparaffinized by submersion in 100% xylene (3 times, 2 min), followed by submersion in declining concentration of ethanol (100% to 75% in four steps) for 2 min. Afterwards the sections were submerged in haematoxylin for 10 min. This was followed by a 30 min wash step using tap water. The sections were then submerged first in Ponceau solution and afterwards in phosphomolybdic acid both for 5 min. To stain collagen the sections were submerged in aniline blue for 8 min which was followed by submersion in phosphomolybdic acid for 5 min. Lastly, the sections were submerged in acetic acid for 1 min. The sections were then dehydrated and mounted with DPX (VWR). Imaging was done with a Nikon Eclipse 80i microscope (Nikon) equipped with a DS-5 M digital camera.

### 2.2.2 Confocal microscopy

L-PRF clots were prepared as described above and fixated overnight at 4°C with 4% paraformaldehyde (PFA) in phosphate-buffered saline (PBS). L-PRF clots were cryoprotected for 96h with 5-30% (w/v) sucrose in PBS, frozen in optimal cutting temperature compound (Tissue-Tek; Sakura Finetek USA, Torrance, CA, USA), and stored at -80°C until further processing. Next, thick sections (about 1 mm in thickness) were prepared by cutting the frozen L-PRF clots with the use of a scalpel blade. Immunostaining were then performed on free-floating L-PRF sections in a 24 well-plate (Greiner Bio-one). The free-floating sections were washed and blocked with 0.2% Triton X-100 and 10% protein block (DAKO, Leuven, Belgium) in PBS for 1h at room temperature (RT). Then, the following primary antibodies were incubated for 48h at 4°C in a humidified chamber: mouse anti-CD41 (1:200, ab11024, Abcam); rabbit anti-fibronectin (1:100 ab2413, Abcam). Following repeated wash steps with 0.2% Triton X-100 in PBS, the L-PRF free-floating sections were incubated with Alexa-labelled secondary antibodies for 24h at RT, namely goat anti-rabbit IgG Alexa 647 and goat anti-mouse Alexa 488 (1:200; all secondary antibodies were obtained from Life Technologies, Merelbeke, Belgium). The specificity of the secondary antibodies was verified by including a control staining in which the primary antibody was omitted (data not shown). A 4',6-diamidino-2-phenylindole (DAPI, Life Technologies) counterstain was performed for 1h at RT to reveal cellular nuclei, and just before imaging the sections were carefully positioned on a long #1.5H coverslips, and covered with a #1.5H coverslip.

Confocal imaging was performed using a LSM 880 Airyscan installed on an inverted Axio Observer (Carl Zeiss, Jena, Germany) and equipped with a long working distance (LD) C-Apochromat 40x/1.1 W (water immersion, Carl Zeiss). Pixel size varied between 0.108 µm and 1.661 µm, measured with pixel dwell times between 1.39 and 3.39 µs per pixel. A series of two sequential, frame-wise alternating scans was used. In the first scan the sample was excited with a 488 nm line of 30-mW air-cooled argon-ion laser (tube current set at 5.9 A) and a 633 nm He-Ne laser, both under the

control of an acousto-optic modulator. This excitation light was directed towards the sample through a dichroic beam splitter (MBS/488/543/633) and the fluorescence was collected through a 1 airy unit pinhole using a GaAsP spectral detector (QUASAR) with a detection band between 490 nm and 588 nm and one between 646 nm and 694 nm for AlexaFluor488 and AlexaFluor647 respectively. The second scan employed non-descanned detection to detect DAPI. A MBS SP 690 beam splitter directed the 810 nm fs-pulsed laser light towards the sample. The emission light was collected using a 690 nm short pass filter and a band-pass (BP) filter, BP 380-430nm. Finally, the signal was registered by a GaAsP photomultiplier tube.

### 2.2.3 Ultrastructural analysis

For SEM examination, L-PRF clots were freshly prepared and immediately fixated in 2% glutaraldehyde at 4°C. After fixation the clots were dried at critical point, dried clots were then broken into smaller pieces. These L-PRF pieces were sputter coated with a thin gold-palladium coat before SEM-imaging took place.

For TEM examination of L-PRF, the clots were fixated with 2% glutaraldehyde in 0.05 M sodium cacodylate buffer (pH 7.3) at 4°C. Following fixation, the clots were post-fixated for 1 h at 4°C with 2% osmium tetroxide in 0.05 M sodium cacodylate buffer (pH 7.3). The clots were then dehydrated with ascending concentrations of acetone (from 50% to 100%). The dehydrated samples were impregnated overnight (O/N) in 1/1 mixture of acetone and araldite epoxy resin (Fluka-Sigma-Aldrich) at RT. The next day the samples were embedded in araldite epoxy resin at 60°C. The samples were then sectioned into semithin (0.5 µm) and thin sections (70 nm) with a EM UC6 microtome (Leica, Wetzlar, Germany). Semithin sections were stained with thionine methylene blue, and imaged with a Nikon Eclipse 80i microscope equipped with a DS-5 M digital camera. Thin sections were transferred to 0,7% formvar-coated copper grids (Aurion, Wageningen, The Netherlands) and contrasted with 0.5% uranyl acetate, lead citrate solution in a EMAC20 contrasting system (Leica). TEM-imaging was done using a EM208 S electron microscope (Philips, Eindhoven, The Netherlands) with a Morada Soft Imaging System camera (Olympus SIS, Münster, Germany) and the corresponding ITEM-FEI software (Olympus SIS, Germany).

## 2.3 Secretome analysis

A secretome analysis was performed to detect the presence growth factors in L-PRF exudate and conditioned medium (CM) collected at different time points as described above. As a first step, we performed an antibody array (Human Cytokine Antibody Array-Membrane, ab133998, Abcam) as a general growth factor screening to identify their presence in the exudate, and the 96h CM "Total CM" of L-PRF. A protein concentration of 10 mg/ml was used in the antibody array. The protein concentrations were determined with the Pierce™ BCA Protein Assay Kit (Thermo Scientific, Erembodegem, Belgium) according to the manufacturer's instructions. The generated chemiluminescent signal from the antibody membranes was detected using a luminescent image

analyzer (ImageQuant LAS 4000 mini). Quantitative analysis was performed on original unmodified blots and densitometry of the protein spots (the relative pixel density of the spots was compared to the positive control set at 100%) was quantified via the ImageQuant TL software. To minimize bias due to differences in densitometric measurements between experiments, each control condition per experiment was set at 100%, thereby lacking a standard error bar.

To ascertain the exact protein concentration of several interesting growth factors an ELISA was performed. The presence of the growth factors BDNF, NT-3, NGF, VEGF-A, PDGF-BB, and GDNF in the exudate, and CM (collected at 24h, 48h, 96h, 144h, and Tot CM) of L-PRF was determined. Six different healthy human donors were tested. The ELISAs for NGF (Boster Biological technology, Boechout, Belgium), and BDNF, NT-3, VEGF-A, PDGF-BB, GDNF (RayBiotech, Boechout, Belgium) were performed in duplicate according to the manufacturers recommendations. Absorbance was measured at 450 nm by an iMark™ Microplate Absorbance Reader (Bio-Rad, Temse, Belgium).

## 2.4 Isolation and stimulation of dorsal root ganglion neurons

DRGs were isolated from female adult Sprague Dawley rats (200-300 g) as previously described (9). Briefly, rats were euthanised with a lethal injection of pentobarbitalnatrium (Dolethal, Vetoquinol, Aartselaar, Belgium). Next, the spinal column was isolated, cut open, and the DRGs were pulled out. The DRG explants were collected in DMEM with 1% P/S. The connective tissue, and nerve roots were removed after which the DRGs were dissociated with a collagenase solution (0,125% for 1.5h at 37°C). After the 1.5h incubation the explants were triturated until a homogenous cell suspension was obtained. The collagenase was then removed from the cells by centrifuging for 10 min at 300g. The cell pellet was resuspended in DMEM with 1% P/S, 10% Foetal Calf Serum (FCS, Lonza, Verviers Belgium) and cytosine arabinoside (Ara-C, 10 µM, Sigma-Aldrich) to deplete non-neuronal cells. The cells were seeded in a poly-D-lysine (PDL)-coated (10 µg/ml, Sigma-Aldrich) 75 $cm^2$ culture flask (Greiner), and placed in a humidified incubator (37°C, 5% $CO_2$) for 24h.

After 24h, the isolated DRGs were enzymatically separated with a trypsin-EDTA solution (0.05%, Thermoscientific). The cells were then centrifuged 6 min at 300g, and the pellet was resuspended in DMEM with 1% P/S. DRGs were plated in a 24 well-plate at a density of 10 000 cell/$cm^2$ on pre-coated coverslips (PDL, 10µg/ml for 1h). The DRGs were serum deprived, and stimulated with exudate (1%, 5%, 10%) and 24h CM (1%, 5%, 10%) (in triplicate) for 72h. Control conditions with either 10% FCS (positive) or 0% FCS (negative) were also included. Furthermore, to check for a potential synergistic effect a condition with 10% FCS and 10% CM was also implemented. During the stimulation cells were placed in a humidified incubator (37°C, 5% $CO_2$). This stimulation was repeated for 6 human L-PRF donors (n=6), 1 rat per donor.

### 2.5.1 Immunofluorescence and neurite outgrowth analysis

After 72h stimulation, DRG neurons were fixated with 4% PFA in PBS for 20 min, and immunostaining were performed as previously described (9). Briefly, the cells were permeabilized with 0.1% triton X-100 in PBS for 15 min followed by a blocking step for 30 min at RT with 10% protein block (DAKO)

in PBS. A primary antibody, mouse anti-Beta Tubulin III (1:400, T8578, Sigma-Aldrich) was added and incubated O/N at 4°C in a humidified chamber. An Alexa-labelled secondary antibody was added namely donkey-anti-mouse Alexa 488 (1: 400, DAM) and incubated at RT for 1h. The cell nuclei were stained with a DAPI (Life Technologies) counterstain for 10 min at RT. The coverslips were then mounted on a microscope slide. Imaging was done with an Eclipse 80i microscope including a digital sight camera DS-2MBWc (Nikon).

For the quantification of the number of cells, neurons and neurites present the NEO-software (DCI-labs), an automated system, was used. The software calculates the amount of neurite outgrowth from the different neurons. The following parameters were used to assess the cell survival, and neurite outgrowth: total number of nuclei, number of neurons, total neurite length, neurite length/neuron, number of neurites/neuron, and number of branches/neurite.

## 2.5 Immunostaining of a ganglion and other cell populations in the DRG culture

DRGs were isolated as previously described. The nerve roots were not removed, and the DRGs were not dissociated. The ganglions were fixated in 4% PFA for 1h. The ganglions were cryoprotected for 96h with 5-30% (w/v) sucrose in PBS, frozen in optimal cutting temperature compound (Tissue-Tek; Sakura Finetek USA, Torrance, CA, USA), and stored at -80°C until further processing. 20µm thick frozen sections of the DRGs were made. Afterwards a staining for mouse anti-Beta Tubulin III was performed as previously described in '2.5.1 Immunofluorescence and neurite outgrowth analysis'.

To check the purity of the DRG culture, immuno-double-staining were performed. These DRGs were also plated, stimulated, and fixated as previously described. Staining was performed as previously described (2.5.1 Immunofluorescence and neurite outgrowth analysis). The following primary antibodies were used: mouse anti-Beta Tubulin III (1:200, Sigma-Aldrich), rabbit anti-S100 (1:200, Z0311, DAKO), rabbit anti-fibronectin (1:200, Abcam), mouse anti-GFAP (1:200, G3963, Sigma-Aldrich); together with the Alexa-labelled secondary antibodies DAM Alexa 488 (1:400) and donkey anti-rabbit Alexa 555 (1:400, DARb)

## 2.6 Animal model of sciatic nerve injury

For this study nine adult female Sprague Dawley rats (200-300 g) (Janvier labs, Le Genest Saint Isle, France) were used. The rats were housed in a conventional animal facility at Hasselt University under controlled conditions such as a temperature-controlled room (20±3 °C), a 12h light-dark cycle, food and water given *ad libitum*. All animal experiments were approved by the local ethical committee of Hasselt University and were performed according to the EU guideline (2010/63/EU) for the protection of animals used for scientific purposes.

Nine rats were randomly divided into three different treatment groups. The first treatment group was the autograft group (n=3). In this group the sciatic nerve was inverted and sutured back in. Secondly there was the empty conduit group (n=3) in which an 8 mm long empty conduit was placed in the

nerve gap. Lastly, there was the L-PRF-conduit group (n=3). For this group the conduit was cut open at one side. The conduit was filled with L-PRF, the sides of the conduit were then sealed again with wound glue (Histoacryl (Braun, Hessen, Germany)). Following this, the conduit was placed in the nerve gap (Figure 3).

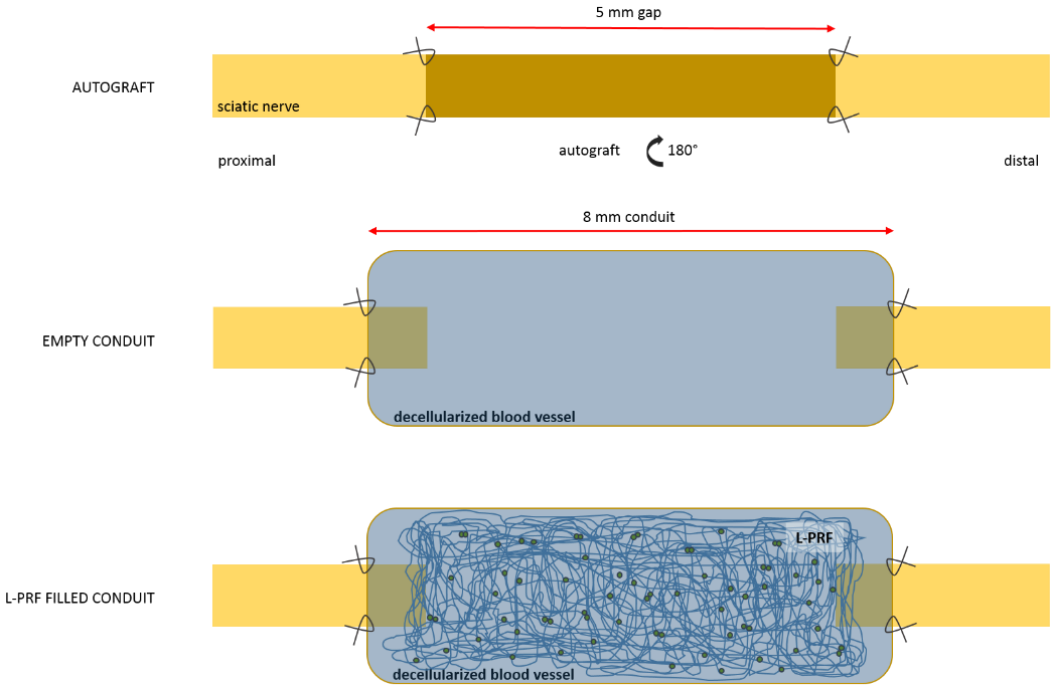


**Figure 3: Representation of the three treatment groups.** The autograft group: a 5 mm piece of nerve is excised and inverted. The empty conduit group: the ends of the nerve are placed in the empty conduit, and sutured in. the L-PRF filled conduit: the conduit is first filled with L-PRF. The nerve ends are then placed in the conduit and the nerves are sutured to the conduit.

The rats were first deeply anesthetised by inhalation of isoflurane (2-4% in $O_2$). Once rats were under anaesthesia the left hind side was shaved, and disinfected with povidone-iodine solution. The sciatic nerve was exposed through a gluteal muscle incision. Once the nerve was exposed, all the connective tissue around the nerve was removed, and a 5 mm piece of the sciatic nerve was cut out. Then rats were treated with the protocol for one of the three treatment groups (mentioned above). After the nerve gap was repaired, the muscle was sewn shut, the skin stapled closed, and the wound was disinfected again with povidone-iodine solution. The rats then received a subcutaneous injection of Buprenorphine (0.1 mg/kg, Temgesic®, MSD, Brussels, Belgium) as post-operative pain relief.

### 2.6.1 Functional recovery

Functional analysis was performed by the Catwalk XT device, an automated walking track analysis system (Noldus, Wageningen, The Netherlands). Animals were trained before the start of the study. Baseline levels were recorded just before the induction of the sciatic nerve injury. Functional recovery

was measured two-weeks post-surgery in all treatment groups. Afterwards the Catwalk software was used to analyse the regularity index (RI), phase dispersions, max contact area, stride length, and swing speed. These parameters were used to assess the functional recovery two weeks after surgery.

### 2.6.2 Histological analysis of the nerves

Two weeks post-surgery all rats received an overdose of pentobarbitalnatrium (Dolethal, Vetoquinol) and were perfused transcardially, first with Ringer solution containing heparin, followed by 4% PFA in PBS. The sciatic nerves, both healthy and injured, were isolated from the rats and put on 4% PFA-5% sucrose solution for 24h. A 2 mm wide piece right in the middle of one conduit/autograft from each treatment group is put on glutaraldehyde (2%), together with one healthy nerve (to make semithin section, see previously mentioned TEM protocol). After 24h the 4% PFA-5% sucrose solution is switched out for 30% sucrose solution for another 72h. The nerves were frozen in optimal cutting temperature compound (Tissue-Tek USA), and stored at -80°C until further processing.

The sections of the nerves were permeabilized with 0.1% triton in PBS for 10 min and then blocked with protein block (DAKO) in PBS for 30 min. The primary antibodies are incubated O/N at 4°C in a humidified chamber. The following primary antibodies were used, mouse anti-Beta Tubulin III (1:250, Sigma-Aldrich), rabbit anti-S100 (1:250, DAKO), rabbit anti-IBA-1 (1:250, #019-19741, Wako, Neuss, Germany). After removal of the primary antibodies, the secondary antibodies GAM Alexa 488 and DARb Alexa 555 (both 1:250) are incubated for 1h at RT. Lastly, the nuclei were counterstained stained with DAPI (Life Technologies) for 10 min, also at RT, and thereafter the sections were mounted. Imaging was done with an Eclipse 80i microscope including a digital sight camera DS-2MBWc (Nikon).

## 2.7 Preparation decellularized blood vessels

As a first step, blood vessels were isolated from the vena saphena of a human cadaver. Afterwards, the blood vessels were decellularized according to a protocol described by Olaussen et al. 2012 (23) with minor modifications. Briefly, the blood vessels were washed with PBS for 72h at 4°C on a shaker. Then they were washed twice with 1% triton X-100 in PBS (3-4h, 37°C on a shaker), followed by a repeated wash step with trypsin/EDTA (3-4h, 37°C on a shaker). Next, the blood vessels were washed with PBS O/N at 37°C also on a shaker. Lastly, the vessels were washed O/N with 4 mg/l deoxyribonuclease I (DNase I) on a shaker at 37°C. All these buffers contained 1% amphotericin b (Fungizone™) and 1% P/S.

After the decellularization process the blood vessels were pulled over a 2 mm wide silicone tube to ensure the inner diameter of the conduits, and frozen quickly on dry ice. The vessels were stored at -80°C until further processing. The frozen blood vessels were then lyophilized and cut to a length of 8 mm.

### 2.7.1 Morphological characterization decellularized blood vessels

The decellularized blood vessels were embedded in paraffin and sectioned (7 µm). Immunofluorescence was performed on the sections. The blood vessels were first deparaffinized as previously described, before they were blocked with 10% protein block (Dako) in PBS for 30 min. The primary antibodies rabbit anti-laminin 1+2 (1:200, Ab7463, Abcam), mouse anti-Human Leukocyte Antigen–antigen D Related (HLA-DR) (1:100, e bioscience (LN3 clone)), rabbit anti-fibronectin (1:200, Abcam) were incubated O/N at 4°C in a humidified chamber. The blood vessels were then incubated for 1h at RT with the following secondary antibodies: GARb Alexa 488 (1:400) and GAM Alexa 555 (1:400) Following this the nuclei were stained with a DAPI (Life Technologies) counterstain before being mounted. Imaging was done with an Eclipse 80i microscope including a digital sight camera DS-2MBWc (Nikon).

The decellularized blood vessels were also analysed by SEM. Both longitudinal, and cross sections were sputter coated with a thin gold-palladium coat before SEM-imaging took place.

Furthermore, the decellularized blood vessels were histologically stained with a Masson's trichome stain. This was done on 5 µm thick paraffin sections. The sections were first deparaffinized and then stained as previously described (2.2.1 Masson's trichome staining).

Lastly, label free imaging, second harmonic generation (SHG) was used to image the blood vessels. 2-photon and confocal microscopy was performed using a LSM 880 Airyscan installed on an inverted Axio Observer (Carl Zeiss) and equipped LD C-Apochromat 40x/1.1 W (Carl Zeiss) or a Plan-Apochromat 20x/0.8 objective (Carl Zeiss). Pixel size varied between 0.130 µm and 1.270 µm, measured with dwell times between 1.02 and 1.26 µs per pixel. Two-photon and confocal microscopy was performed by means of two sequential, frame-wise alternating scans. For the two-photon scan, the excitation was provided by a femtosecond pulsed laser (MaiTai DeepSee, Spectra-Physics, CA, USA) tuned to a central wavelength of 810 nm controlled by an EOM. Both the SHG signal and and autofluorescence were collected by the objective in backward mode, separated from the excitation light by a 690 nm short pass dichroic mirror, and separated from each other by a 442 nm dichroich mirror. After passing through respectively a 400-410 nm band pass filter and a 450-650 nm band pass filter, the SHG signal and autofluorescence were simultaneously recorded using GaAsP photomultiplier tubes operating in analogue mode. In the second scan, the fluorescence of AlexaFluor 488 was detected. Excitation occurred with a 488 nm line of 30-mW air-cooled argon-ion laser (tube current set at 5.9 A) under the control of an acousto-optic modulator. This excitation light was directed towards the sample using a MBS 488 dichroic mirror. The resulting fluorescence was collected through a 1 airy unit pinhole using a GaAsP spectral detector (QUASAR) with a detection band between 490 nm and 588 nm.

## 2.8 Statistical analysis

Statistical analysis as performed using GraphPad Prism 7 software (GraphPad, San Diego, CA, USA). All data was first subjected to a D'Agostino–Pearson normality test. The data from the neurite

outgrowth analysis was compared by a Kruskal-Wallis test followed by a Dunn's multiple comparisons post hoc test. Values of $P < 0.05$ were considered statistically significant. All data was expressed as ± standard error of the mean (SEM). All analysis in this study was done on the original un-processed figures, however for better visibility the contrast was enhanced for the representative figures shown.

# 3. Results

## 3.1 Defining the morphological structure of L-PRF

As a first step, we examined the morphological structure of L-PRF in more detail. Therefore, several different techniques were performed to get a detailed picture of L-PRF. First, we performed a trichrome staining to characterize the different areas of L-PRF (Figure 4A, B, C). Based on the trichrome staining, we can distinguish two morphological areas in L-PRF, namely the fibrin matrix, and the cell-rich area (Figure 4A). We observed that the cell-rich area consists out of blood cells which are most likely to be leukocytes, and red blood cells (Figure 4B), while the fibrin matrix consists out of randomly organized fibrin fibres (Figure 4C) Next, we verified the observations found in the histological staining. This was done with a staining for fibronectin and CD41 (blood platelets), imaged with a confocal microscope. The same two areas of L-PRF seen earlier could be observed. The platelet-rich zone divides the fibrin matrix, and the cell-rich area from each other. This platelet-rich zone consists out of tightly packed blood platelets which is interrupted by cells from the cell rich area (Figure 4D). We also determined that the fibrin matrix is more densely organized along the border of the clot, however, in the rest of the L-PRF clot the density of the fibres remains about the same. Additionally, we found that many blood platelets are located in the fibrin matrix (Figure 4E).

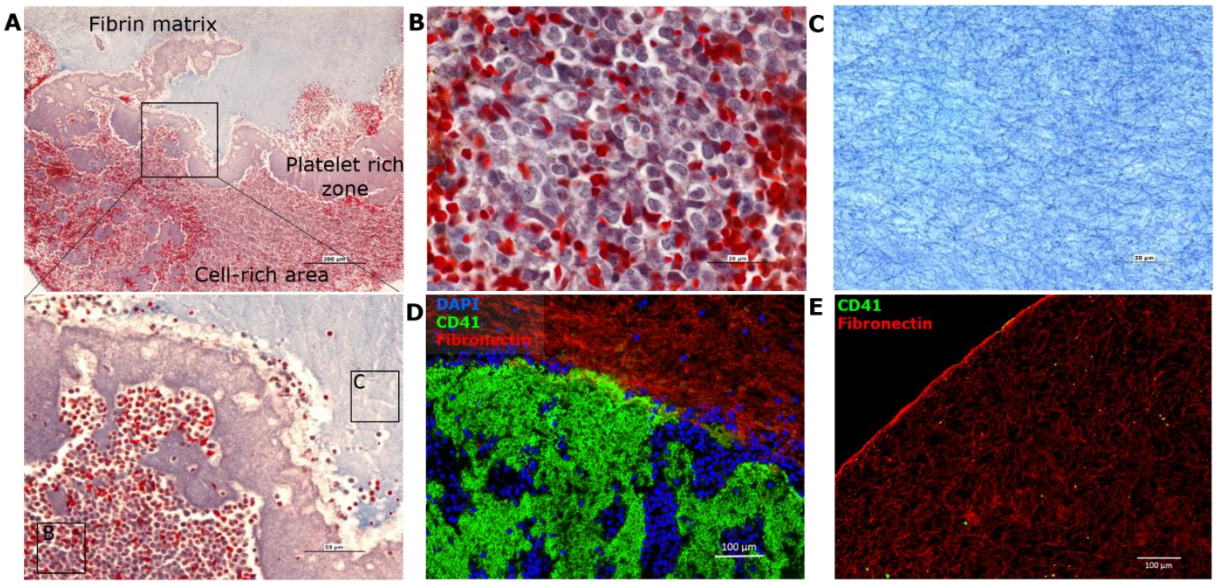


**Figure 4: Leukocyte- and Platelet-Rich Fibrin (L-PRF) consists out of two morphological distinguishable structures. (A)** A Masson's trichrome staining was performed on L-PRF. Two different morphological areas can be distinguished, namely the fibrin matrix, and the cell-rich area which are separated by a platelet-rich zone. (scale: 200µm→50µm) **(B)** Enlargement of (A) showing the cell-rich area of L-PRF. All the cells present are blood cells, most likely leukocytes and red blood cells. (scale: 20µm) **(C)** Enlargement of (A) showing the fibrin matrix. The densely packed fibrin fibres can be observed. (scale: 20µm) **(D)** Confocal tile-scan of L-PRF stained for fibronectin, DAPI (nuclei) and CD41 (blood platelets). The two morphological areas of L-PRF can be distinguished. Fibronectin shows the fibres of the fibrin matrix. The platelet rich zone consists out of an immense amount of blood platelets packed tightly together. Islands of blood platelets are surrounded with cells from the cell-rich area, this was also visualized by the trichome staining (A). **(E)** Confocal tile-scan of the fibrin matrix stained for fibronectin and CD41 (blood platelets). Some blood platelets can be seen in the fibrin matrix. Along the border of the clot, the fibrin matrix is organized much more densely.

As a next step we analysed the ultrastructure of L-PRF with SEM-imaging. Ultrastructural analysis showed that the fibrin fibres are very thin, less than 1 µm, and that these fibres are tightly interwoven with each other (Figure 5A). Furthermore, we observed that the cell-rich area contained a lot of red blood cells, recognisable by their distinct biconcave shape (Figure 5B). The red blood cells are located close together imbedded in the fibrin fibres.

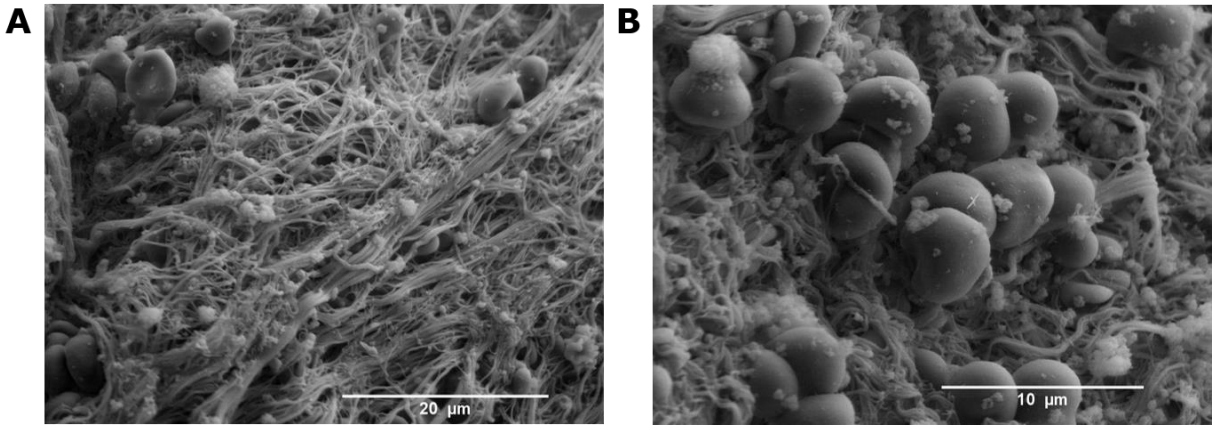


**Figure 5: L-PRF contains very thin fibrin fibres and many red blood cells. (A)** Scanning electron microscopic (SEM) image of a fibre rich area in L-PRF. The thin, randomly organised fibres form a tight matrix. **(B)** SEM image of the cell-rich area of L-PRF showing the presence of many red blood cells recognisable by their biconcave shape.

As a next step, we aimed to characterize the organization of the fibrin matrix. Therefore, we performed an immunostaining for fibronectin and CD41 (blood platelets). This was visualized by confocal microscopy to accurately define the 3D-structure of the clot. From these images we can confirm that L-PRF consists of a dense network of fibrin fibres which are randomly orientated (Figure 6A, B). As mentioned before, the fibrin matrix becomes denser along the border of the clot. However, the L-PRF remains very porous. Additionally, the blood platelets present in the clot form large clusters (Figure 6C, D). In the middle of the fibrin matrix, we observed more randomly distributed clusters of activated platelets. Furthermore, the density of the fibrin matrix increases in the vicinity of these activated platelets (Figure 6E, F).

We also characterized the cellular content of L-PRF by ultrastructural analysis via TEM. The blood platelets in the L-PRF fibrin matrix were found to be tightly packed together. Moreover, we observed that all blood platelets present were activated (all inner granules have been released from the cell) (Figure 7A). These clusters of activated blood platelets are surrounded by a dense network of fibrin fibres (Figure 7B). In the cell-rich area of L-PRF, we determined that there was a high presence of leukocytes, and red blood cells. In this area, only a few fibrin fibres could be observed (Figure 7C).

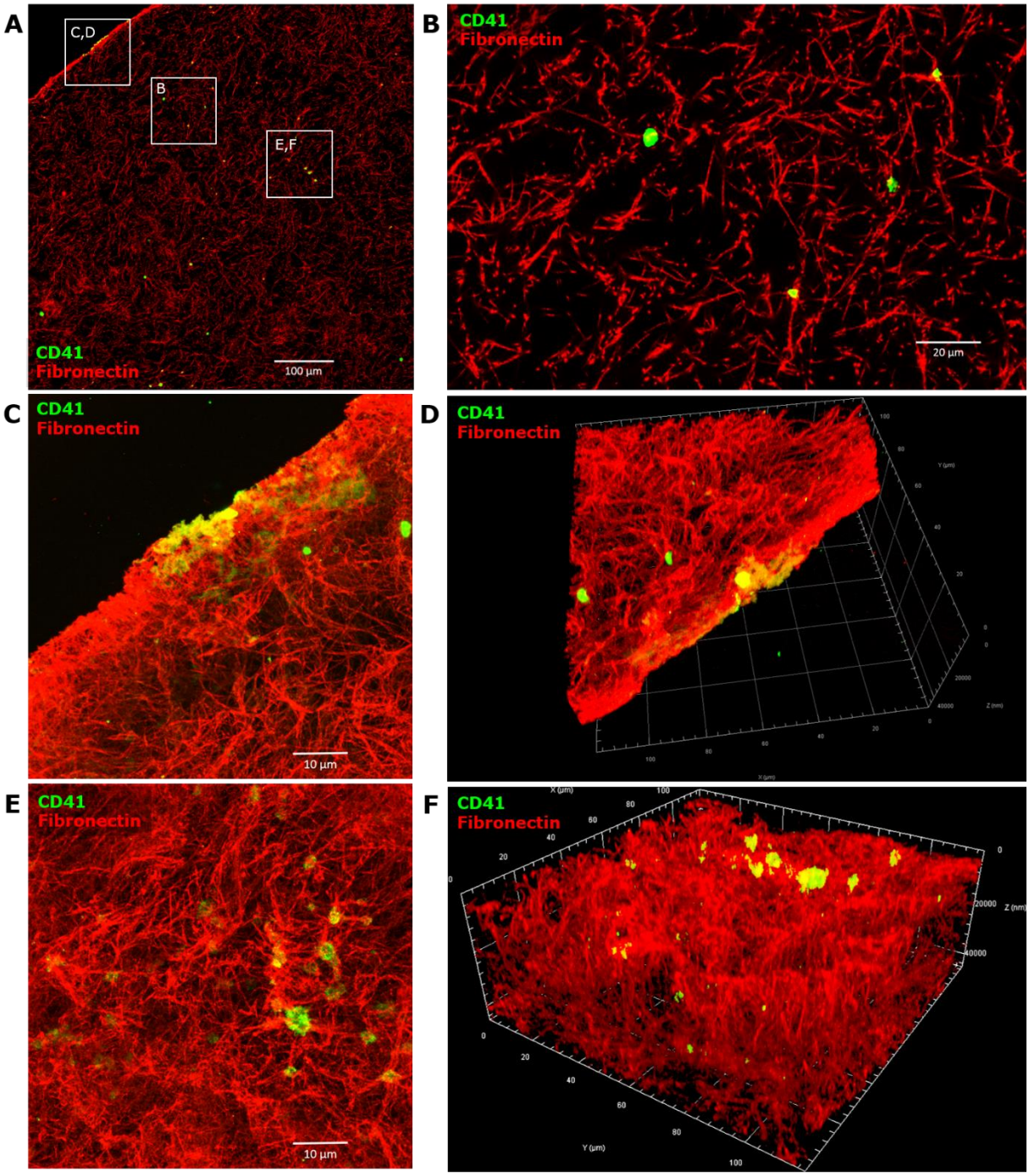


**Figure 6: The fibrin matrix of L-PRF is porous and consists out of randomly organised fibres in which clusters of blood platelets are located.** Confocal imaging of L-PRF stained for fibronectin and CD41 (blood platelets). **(A)** Tile scan of the fibrin matrix. The squares mark an area where either an optical section (B) or a Z-stack (C-F) was taken. **(B)** Thin optical section of the L-PRF fibrin matrix showing randomly organized fibrin fibres. **(C, D)** A Z-stack was made along the border of the clot. Max intensity projection of the Z-stack (C), along with a 3D-projection of the same stack are shown (C). Fibres in the fibrin matrix are more densely organized around the border of the clot and the platelets. **(E, F)** A Z-stack was made in the middle of the L-PRF fibrin matrix. The max intensity projection of Z-stack (E), along with a 3D-projection (F) of the same stack are shown. The blood platelets form clusters in the fibrin matrix and these fibres are organized much more densely around these clusters. Overall, the fibrin matrix is very porous.

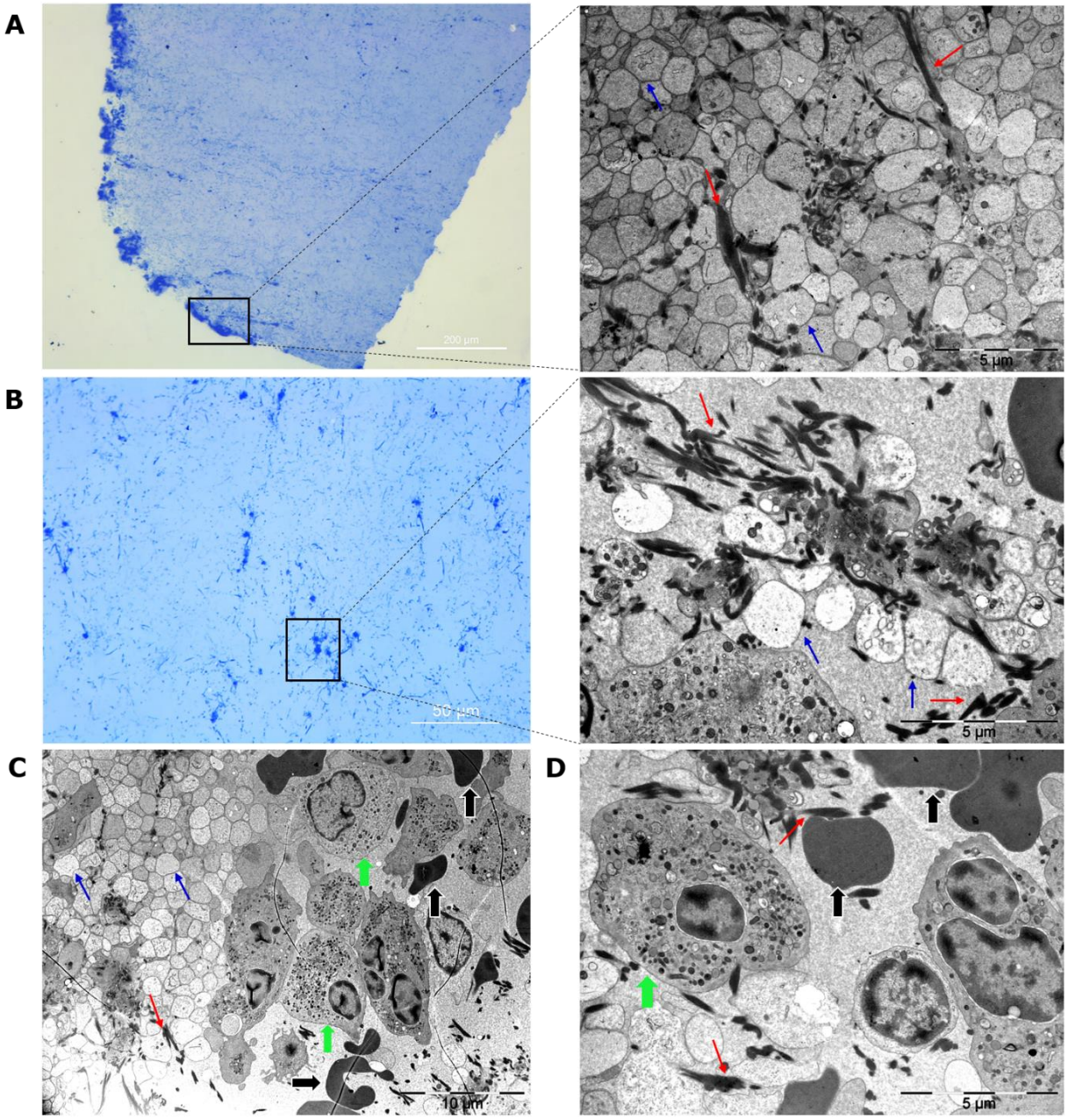


**Figure 7: Leukocyte- and Platelet-Rich Fibrin (L-PRF) contains activated blood platelets, leukocytes, and red blood cells surrounded by fibrin fibres.** Ultrastructural analysis of L-PRF was done by transmission electron microscopy (TEM). **(A)** Semi-thin section of L-PRF, the square marks the approximate area where the TEM image was taken. The TEM-image shows tightly packed blood platelets surrounded with a lot of fibrin fibres. **(B)** Semi-thin section of L-PRF, the square marks the approximate area where the TEM image was taken. The TEM-image shows a cluster of blood platelets surrounded by many fibrin fibres. **(C, D)** TEM-images showing tightly packed activated blood platelets, leukocytes, and red blood cells. Between these cells some fibrin fibres are present. (Blue arrows = blood platelets, red arrows = fibrin fibres, green arrows= leukocytes, black arrows = red blood cells)

## 3.2 L-PRF is a reservoir for a plethora of growth factors and cytokines

Next, this study focused on investigating the growth factor release from L-PRF over time. First, an antibody array was performed as a general screening of the growth factors released by L-PRF. This technique is able to screen for 80 different proteins simultaneously. The array was performed on exudate and CM (collected after 96h) from four different donors, and the protein expression of all

the detected growth factors is illustrated in the heat map (Figure 8A). The analysis showed high protein levels of PDGF-BB in both the exudate and CM of two donors. PDGF-BB was also detected in the other two donors but the relative protein levels were much lower. VEGF was abundantly present in the CM of one donor while one other donor showed no VEGF release in its CM. Furthermore, the other donors had low levels of VEGF in their CM, similar to the levels of VEGF found in the exudate of all four donors. The release of BDNF was only found in three donors. These three donors had minor levels of BDNF in the exudate, and only two donors had low levels of BDNF in the CM. Only two donors were found to have low levels of the growth factors GDNF and NT-3 in the exudate and CM. No GDNF nor NT-3 were detected in the other two donors. The data obtained from the antibody array also shows that there is a lot of variation in protein levels between donors, and between the exudate and CM for certain factors.

Several growth factors detected in the antibody array, like NT-3, GDNF, BDNF can be beneficial for nerve regeneration. Therefore, the levels of these growth factors along with VEGF, NGF, and PDGF released from L-PRF were quantified by ELISA. The exact growth factor concentrations were analysed in the exudate, and CM at 24h, 48h, 96h, and 144h to assess the release of the factors over time. PDGF protein levels in the exudate (647.11 pg/ml ± 23.82) were found to be in the same range as those detected in the CM after 144h in culture (549.84 pg/ml ± 71.62) (Figure 8C). After 24h the release of the protein peaked (970 pg/ml ± 40.99) after which the release of the protein lowered slowly at the next time points. However, after 144h the protein was still released from L-PRF.

A similar pattern of release was observed for BDNF, namely a peak in the release of the factor after 24h (Figure 8D). BDNF protein levels were detected in relatively low concentrations in the exudate (8.45 ng/ml ± 3.00) compared to the CM. After 24h in culture, we observed a strong release of BDNF in the medium (89.11 ng/ml ± 3.95) and these protein concentrations decreased gradually over time. It is important to note that even after 144h BDNF protein levels were still detected in the medium. Overall the BDNF protein concentrations were much higher compared to the other growth factors assessed by ELISA in this study.

In contrast to both PDGF and BDNF, protein concentrations of NGF gradually increased in time peaking at 96h (623.66 pg/ml ± 119.34) (Figure 8E). The exudate was found to have the lowest concentration (30,14 pg/ml ± 7.12). Even though, the highest concentration was detected after 96h, the protein was still released after 144h at a reasonably high concentration (433.16 pg/ml ± 13.98). The release pattern of VEGF was comparable to that of NGF (Figure 8F). The exudate had the lowest release (18.46 pg/ml ± 5.49), and the proteins levels increased in the CM with peak levels after 96h (149.16 pg/ml ± 24.86). VEGF was still detectable in the medium after 144h (120.20 pg/ml ± 13.51).

Both NT-3 and GDNF were only detected in one of the six donors tested, which indicates that there is variability between donors (as observed in the antibody array). Moreover, NT-3 and GDNF protein levels were only detected in the exudate and 24h CM of this donor (Figure 8G). The highest concentrations were detected in the exudate (NT-3: 152.90 pg/ml; GDNF: 143.90 pg/ml), while only a low protein release was found after 24h (NT-3: 17.42 pg/ml; GDNF: 6.81 pg/ml).

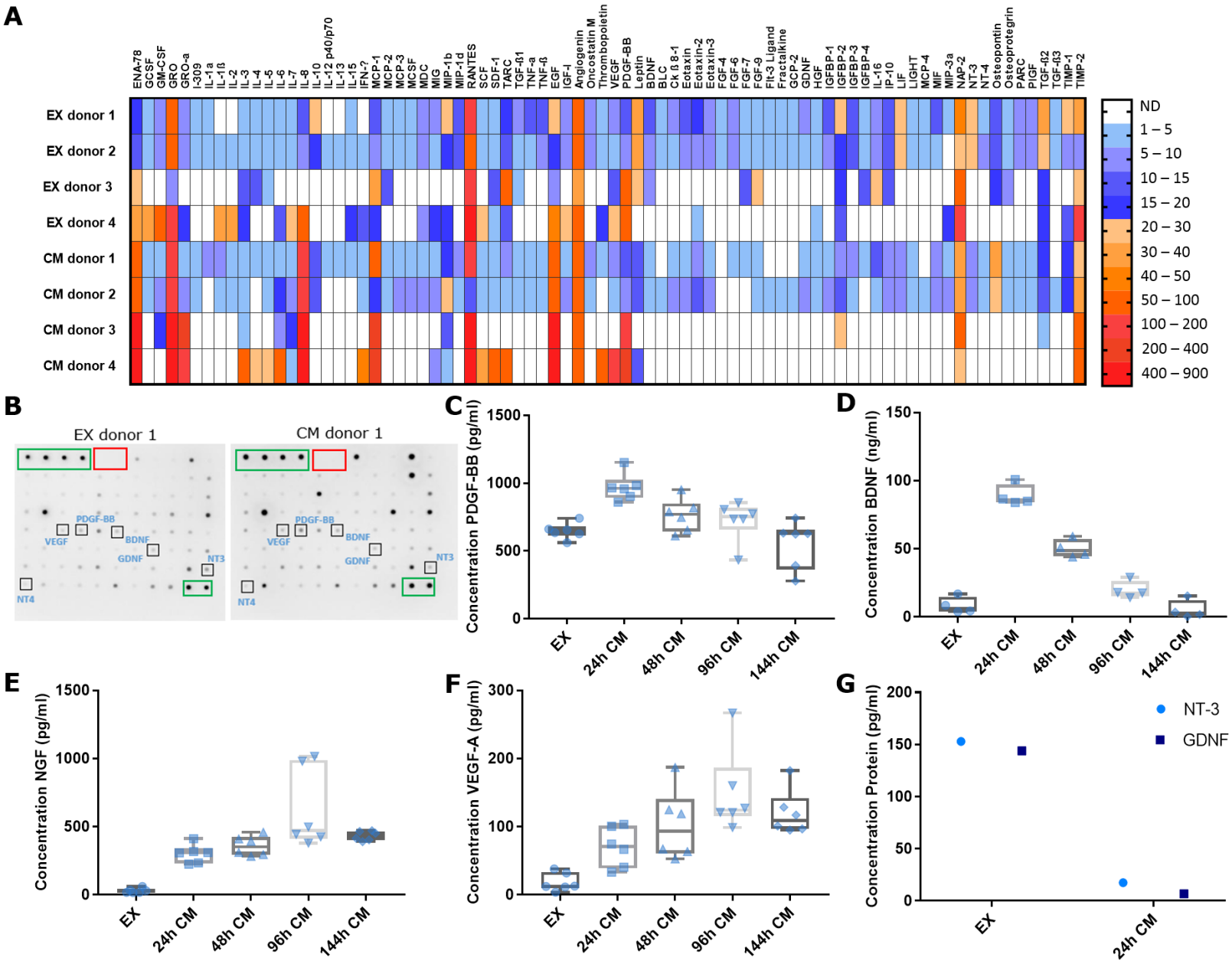
A
ENA-78
GCSF
GM-CSF
GRO
GRO-a
I-309
IL-1a
IL-1ß
IL-2
IL-3
IL-4
IL-5
IL-6
IL-7
IL-8
IL-10
IL-12 p40/p70
IL-13
IL-15
IFN-?
MCP-1
MCP-2
MCP-3
MCSF
MDC
MIG
MIP-1b
MIP-1d
RANTES
SCF
SDF-1
TARC
TGF-ß1
TNF-a
TNF-ß
EGF
IGF-I
Angiogenin
Oncostatin M
Thrombopoietin
VEGF
PDGF-BB
Leptin
BDNF
BLC
Ck ß 8-1
Eotaxin
Eotaxin-2
Eotaxin-3
FGF-4
FGF-6
FGF-7
FGF-9
Flt-3 Ligand
Fractalkine
GCP-2
GDNF
HGF
IGFBP-1
IGFBP-2
IGFBP-3
IGFBP-4
IL-16
IP-10
LIF
LIGHT
MCP-4
MIF
MIP-3a
NAP-2
NT-3
NT-4
Osteopontin
Osteoprotegrin
PARC
PIGF
TGF-ß2
TGF-ß3
TIMP-1
TIMP-2
EX donor 1
EX donor 2
EX donor 3
EX donor 4
CM donor 1
CM donor 2
CM donor 3
CM donor 4
ND
1 – 5
5 – 10
10 – 15
15 – 20
20 – 30
30 – 40
40 – 50
50 – 100
100 – 200
200 – 400
400 – 900
B
EX donor 1
CM donor 1
PDGF-BB
VEGF
BDNF
GDNF
NT3
NT4
C
Concentration PDGF-BB (pg/ml)
1500
1000
500
0
EX
24h CM
48h CM
96h CM
144h CM
D
Concentration BDNF (ng/ml)
150
100
50
0
E
Concentration NGF (pg/ml)
F
Concentration VEGF-A (pg/ml)
300
200
100
G
Concentration Protein (pg/ml)
NT-3
GDNF

**Figure 8: Leukocyte- and Platelet-Rich Fibrin (L-PRF) releases a plethora of growth factors and cytokines. (A)** Heatmap illustrating the presence of 80 different proteins in exudate (EX) and conditioned medium (CM, collected after 96h) of L-PRF, which was analysed by an antibody array (n=4). **(B)** Representative antibody array blots incubated with either EX or CM (collected after 96h) from one donor. The location of several interesting proteins is marked on the blots, such as vascular endothelial growth factor (VEGF), platelet derived growth factor-BB (PDGF-BB), brain derived neurotrophic factor (BDNF), glial-derived neurotrophic factor (GDNF), neurotrophin (NT)-3, and -4 **(C-G)** The protein concentrations of PDGF-BB, BDNF, NGF, VEGF-A, NT-3, and GDNF determined by ELISA. L-PRF protein release was tested in the EX and CM collected at 24h, 48h, 96h, and 144h. The individual protein concentrations from each donor are represented as separate dots in the graph**.** Because of the large variation in the samples, the protein concentrations for NT-3, and GDNF were only detectable in 1 of the 6 donors. The measured growth factors are slowly released from L-PRF over time. Most growth factors are still released after 144h. (n=4-6).

## 3.3 L-PRF stimulates neurite outgrowth of DRG neurons *in vitro*

As a next step, we investigated the effect of L-PRF on the survival, and neurite outgrowth of primary rat DRG neurons. The DRGs were stimulated for 72h with the following conditions: serum deprived medium (control), with 10% FCS (positive control) and with varying concentrations of L-PRF exudate (1%, 5%, 10%), and CM (1%, 5%, 10%) (Figure 9). Cells were stained for BIII tubulin, and cell survival and neurite outgrowth was analysed by using the NEO software. We observed that that the cell survival (Figure 9A, B), and more specifically the survival of DRG neurons (Figure 9A, C) was significantly improved ($P < 0.0001$) in the conditions that received 1%, 5% or 10% CM compared to the control condition. Furthermore, compared to the control (serum deprived), we observed that the DRGs stimulated with the CM (1%, 5%, 10%) had a significant ($P < 0.0001$) dose-dependent increase in the overall neurite outgrowth. This was shown by the increase in the total neurite length (Figure 9D), neurite length per neuron (Figure 9E), number of neurites per neuron (Figure 9F), and number of branches per neurite (Figure 9G). In contrast, we did not observe these effects on cell survival and neurite outgrowth in DRGs stimulated with L-PRF exudate.

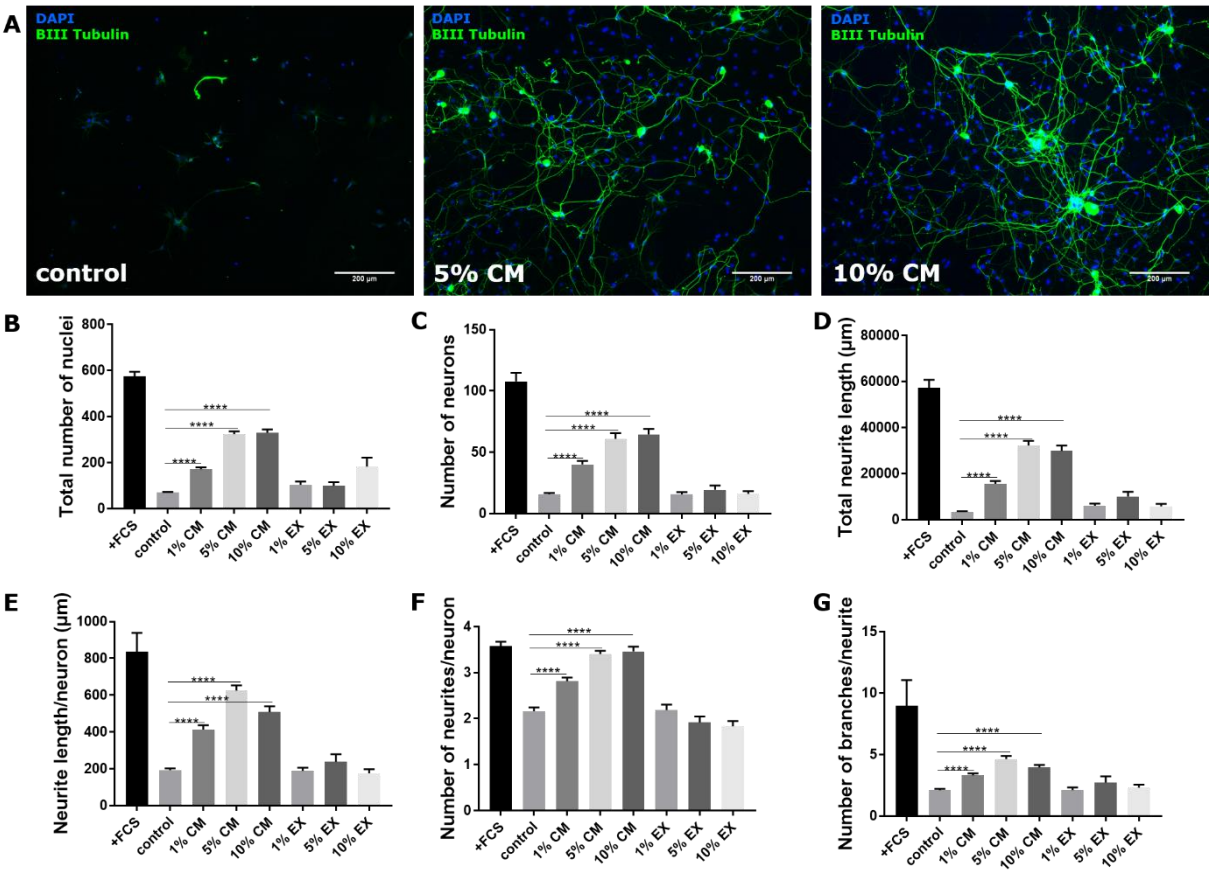


**Figure 9: Growth factors present in conditioned medium of Leukocyte- and Platelet-Rich Fibrin stimulate cell survival and neurite outgrowth *in vitro*.** Primary rat dorsal root ganglion (DRG) neurons were stimulated for 72h with different concentrations of L-PRF exudate (EX) and conditioned medium (CM) (1%, 5%, 10%). Also, control conditions with 10% FCS (+FCS) or serum deprived (control) were included in this experiment. **(A)** Representative photomicrographs of DRG neurons stimulated with L-PRF CM, the control and experimental conditions CM 5% and 10% are shown. (BIII tubulin positive neurons = green; DAPI positive nuclei = blue). **(B-G)** Immunofluorescence for BIII tubulin (positive neurons) was performed, and cell survival and neurite outgrowth were analysed using the NEO software**.** All CM conditions give a significantly improved effect on the cell survival, and neurite outgrowth when compared to the control. However, no significant differences are observed between the exudate conditions and the control. (****= P < 0.0001, analysed with the Kruskal-Wallis test and Dunn's multiple comparisons post-hoc)

We observed that only a small percentage the of cells in our culture were neurons (Figure 10A, B, C). Therefore, as a next step the purity of the cell culture was assessed; we performed several immunofluorescent staining to identify the other cell population that was present in our DRG culture. A S100-BIII tubulin-staining was performed to identify SCs, and neurons present in the culture (Figure 10A). A large amount of SCs were found to be present in the primary cultures. Surprisingly, we observed that most SCs align with the neurites, highlighting their supportive function. Furthermore, we also stained for fibronectin to detect whether fibroblasts are present in our culture system, and we detected some fibronectin-positive cells (Figure 10B). Additionally, we performed a GFAP-staining combined with a fibronectin-staining where we determined that the fibronectin positive cells are also GFAP-positive, thereby identifying these cell as SCs (Figure 10C).

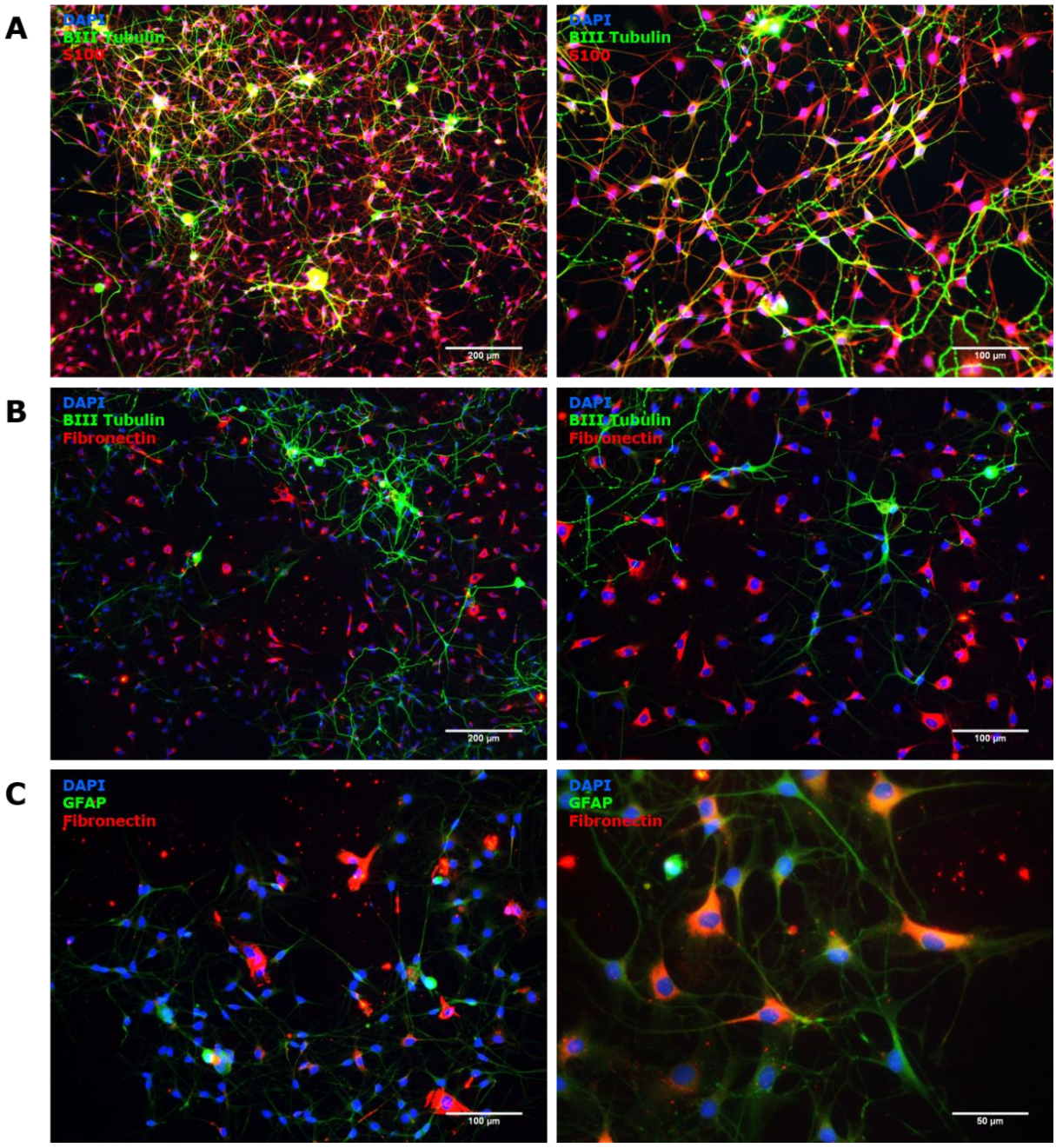


**Figure 10: Mixed neuronal cell cultures consist of BIII tubulin positive neurons, and S100 positive Schwann cells.** Immunofluorescence staining were performed for BIII tubulin, S100, fibronectin, and GFAP to assess the purity of the neuronal cell cultures. **(A)** Image of a DRG culture showing the presence of Schwann cells (SCs) (S100) together with the neurons (BIII tubulin). There is a numerous amount of SCs present in the culture**. (B)** Imaging of Fibronectin-positive cells which might indicate the presence of fibroblasts in the culture in between the neurons (BIII tubulin). **(C)** Imaging of glial fibrillary acidic protein (GFAP) -positive cells together with fibronectin, shows that the fibronectin-positive cells are SCs.

## 3.4 Pilot study, rat sciatic nerve injury model

A pilot study using a rat sciatic nerve injury model was set up to study the effect of L-PRF on the nerve regeneration *in vivo*. We decided to use the sciatic nerve because it is the largest nerve, and composed out of both myelinated and unmyelinated axons (Figure 11A-C). The nerve injury was induced in the left hind limb of the rats by transecting a 5 mm piece of the sciatic nerve (Figure 11D). Three different treatment groups were used in the nerve injury model, the autograft group (Figure E), the empty conduit group (Figure 11F, G), and the L-PRF filled conduit group (Figure 11F, G).

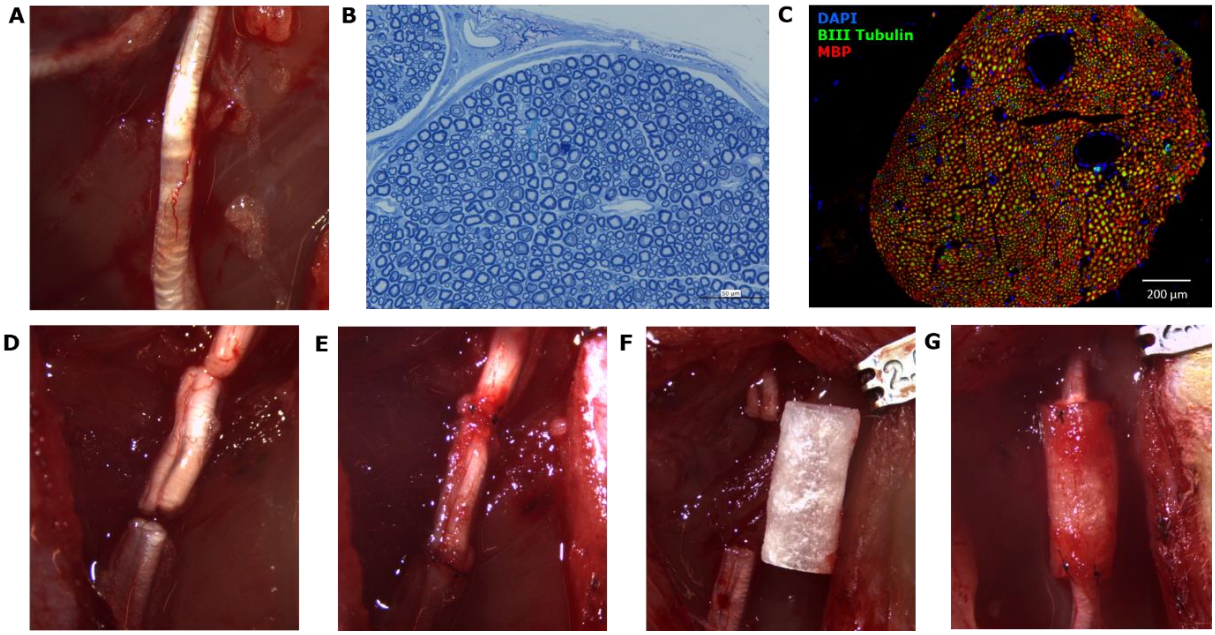


**Figure 11: Inducing large gap sciatic nerve injury in Sprague Dawley rats. (A)** An exposed healthy sciatic nerve. **(B)** Semi-thin section of a healthy sciatic nerve showing myelinated and unmyelinated axons. The axons are surrounded by the perineurium, and epineurium (scale: 50 µm) **(C)** Fluorescent staining for BIII tubulin (axons), and myelin basic protein (MBP, myelin) in a healthy sciatic nerve. Most axons are fully surrounded by myelin. **(D)** A sciatic nerve where a 5 mm piece of the nerve has been transected. **(E)** An autograft of the sciatic nerve, the nerve has been inverted and sutured back in. **(F)** The implantation conduit. The conduit is longer than the gap so that the ends of the nerves can be placed in the conduit**. (G)** A large gap sciatic nerve injury bridged with a conduit (either with or without L-PRF). The nerve ends are placed in the conduit and sutured in place.

During the *in vivo* study, functional recovery of the rats was examined by analysing different gait parameters using the Catwalk system (Figure 12A). Baseline measurement of the rats were compared to measurement taken two weeks post-surgery. The regularity index (RI) and phase dispersions both give information on interlimb coordination (Figure 12B). Both these parameters were decreased after nerve injury indicating a diminished limb coordination in all three treatment groups when compared to baseline levels. Two weeks post-surgery, we observed that the nerve injury also affected movement of the left hind limb. The previous observation was made based on the lower max contact area, the shorter stride length and the slower swing speed of the left hind limb (Figure 12B).

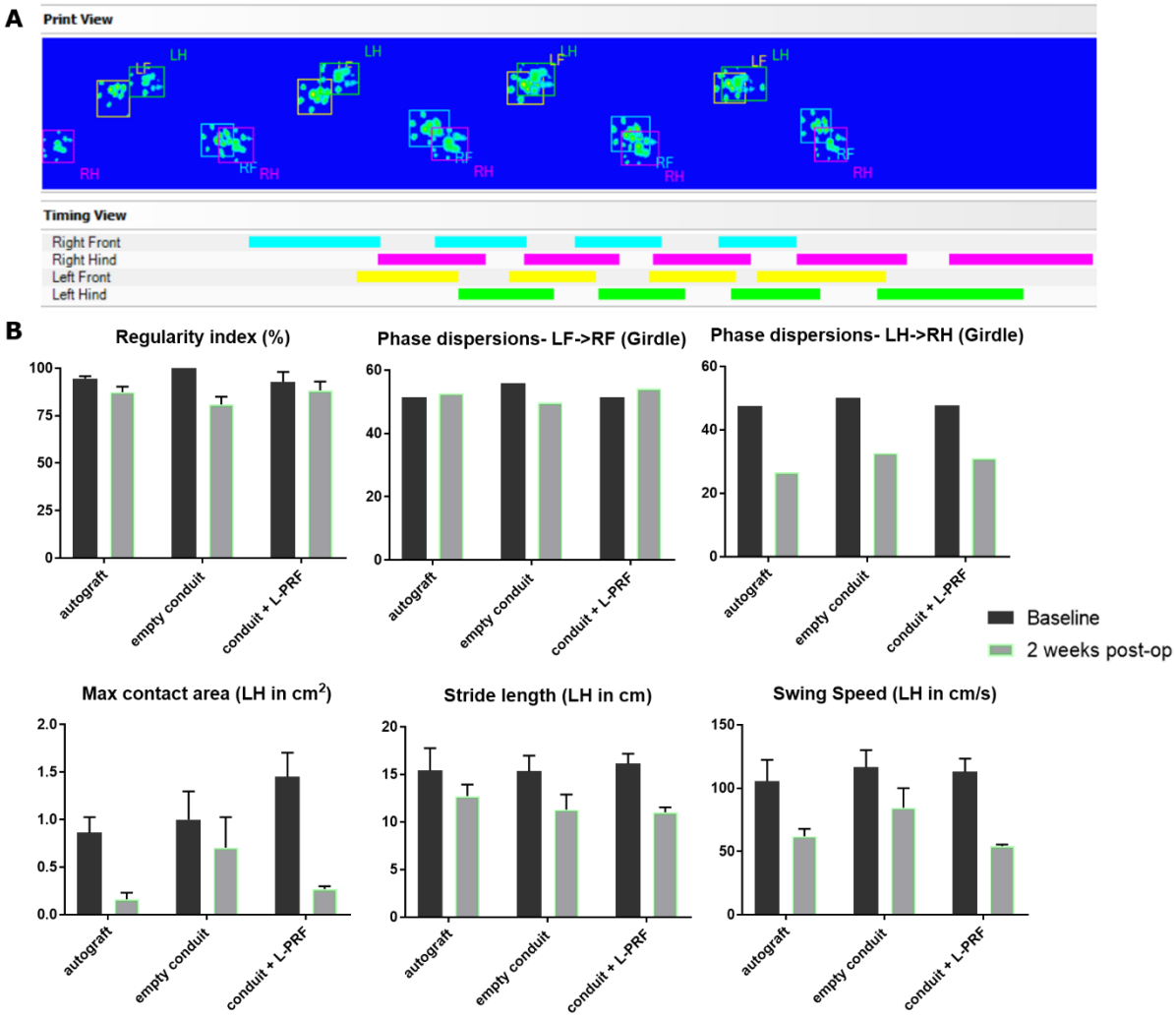


**Figure 12: Rats with a sciatic nerve injury lose their hind paw coordination.** Sciatic nerve injury was induced in rats, for the three different treatment groups (autograft, empty conduit and L-PRF + conduit), baseline functional recovery measurements where compared to measurements taken two weeks post-surgery. **(A)** Representation of paw prints measured by the catwalk. **(B)** Functional analysis of the rats. The regularity index seems to be lower two weeks after surgery. The walking pattern of the rats are thus less coordinated. The phase dispersion of the hind paws indicates a limp by the lower values measured after injury. Two weeks post-surgery the rats do not place their left hind paw completely down on the surface of the runway (max contact area), and both the stride length and the swing speed of the left hind limb are shorter.

After the two-week follow-up period, the cell infiltration into the proximal end of the nerve lesions was assessed in all three functional groups. A S100-DAPI-staining was performed on cross sections of the nerves to identify the amount of cells (DAPI), and SCs (S100) present in regenerating nerve. A healthy nerve was included to serve as control (Figure 13). We observed that all injured nerves, regardless of which treatment group, had a massive cell infiltration (DAPI) (Figure 13). Furthermore, it seemed that only a few SCs (S100) infiltrated in the L-PRF filled conduit group, however further analyses, and quantification are needed to confirm this. In contrast, the other two treatment groups had a large SC infiltration (Figure 13). Moreover, we observed that a lot of cells present in the injured nerves (all treatment groups) are not SCs (Figure 13, Merged image). Some of these other cells were confirmed to be macrophages (staining for IBA-1) (data not shown).

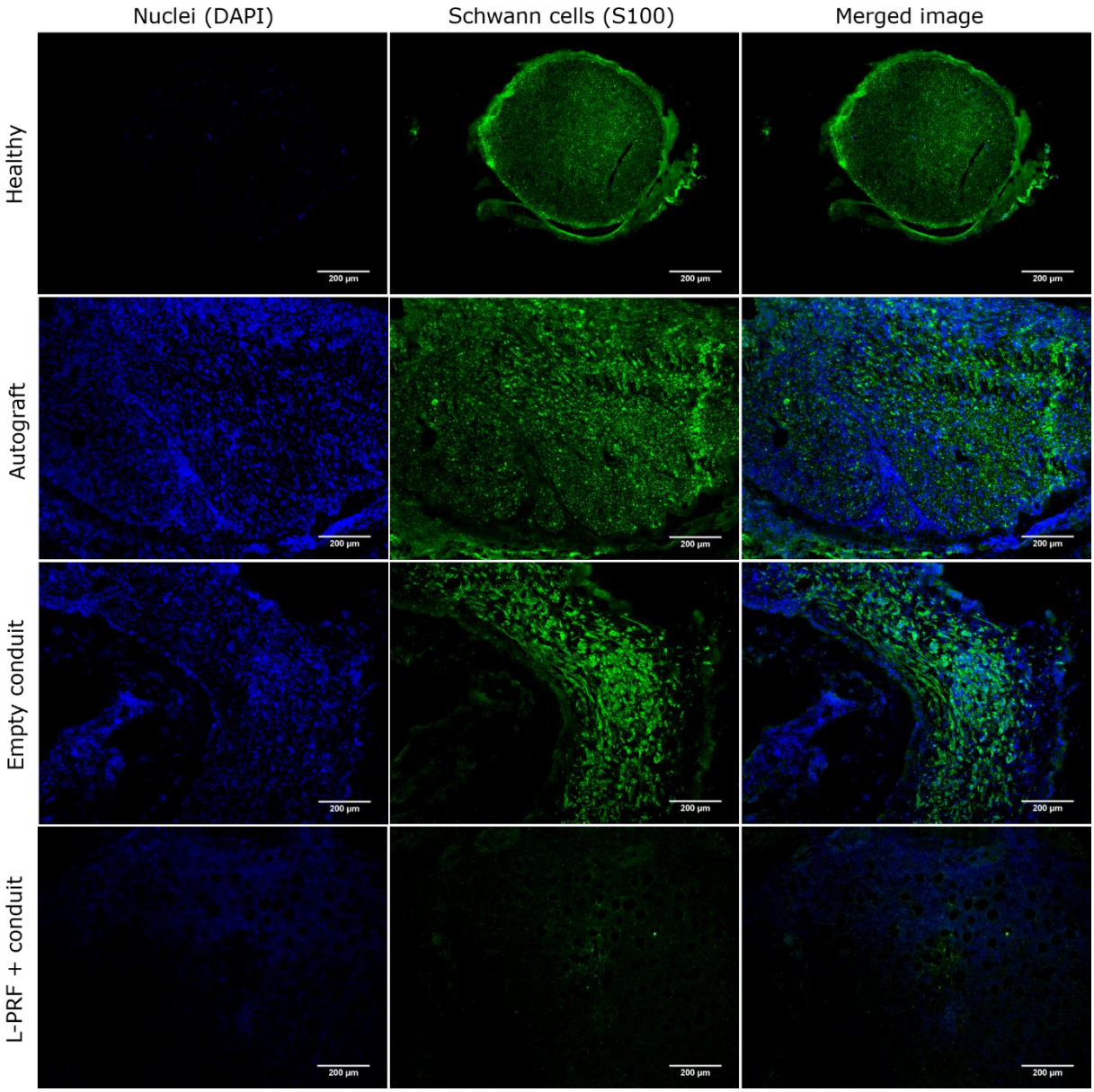


**Figure 13: Infiltration of S100+ Schwann cells in the transplant area two weeks post injury.** Representative cross sections from the proximal end of the nerve are shown for all treatment groups (autograft, empty conduit, L-PRF conduit), nuclei labelled with DAPI (blue) and S100 positive Schwann cells (green). Images of a healthy nerve were included as a control. All treatment groups show a lot of cell infiltration when compared to a healthy nerve. All treatment groups have SCs infiltration.

### 3.4.1 Decellularized blood vessels as suitable conduits for nerve repair

To implant L-PRF between two nerve endings we chose to use decellularized blood vessels as a supporting structure. Here we characterized whether our decellularization process was successful. An important requisite for a conduit is that it doesn't induce any immune reactions as this would not be beneficial for the regeneration. It is crucial that all foreign antigens are removed, therefore, it an immunostaining (for HLA-DR) verified that no HLA-DR, a MHC class II cell surface receptor, was present in the conduit (data not shown). Staining for cell nuclei also proved that all cells had been removed from the vessel (data not shown). Next, we performed detailed microscopic analysis to verify that the supporting ECM was still intact. We observed that the ECM was preserved, and that it

formed a hollow tube with a consistent inner diameter of 2 mm (Figure 14B). We also performed a trichome staining, and label-free optical imaging techniques, namely SHG and autofluorescence, to further study the decellularization of the blood vessel. We verified that all cells were removed from the vessel wall, and only the ECM structure remained (Figure 14C-G). Furthermore, collagen type I (SHG) is located mainly on the outer side of the conduit while the inner side of the conduit has a lot of autofluorescence, which potentially originates from elastin (Figure 14E, F). However, we have to confirm this by immunostaining in the future. The ECM-component fibronectin was also still present in the vessel wall, and interestingly located on similar positions as the autofluorescence (Figure 14G).

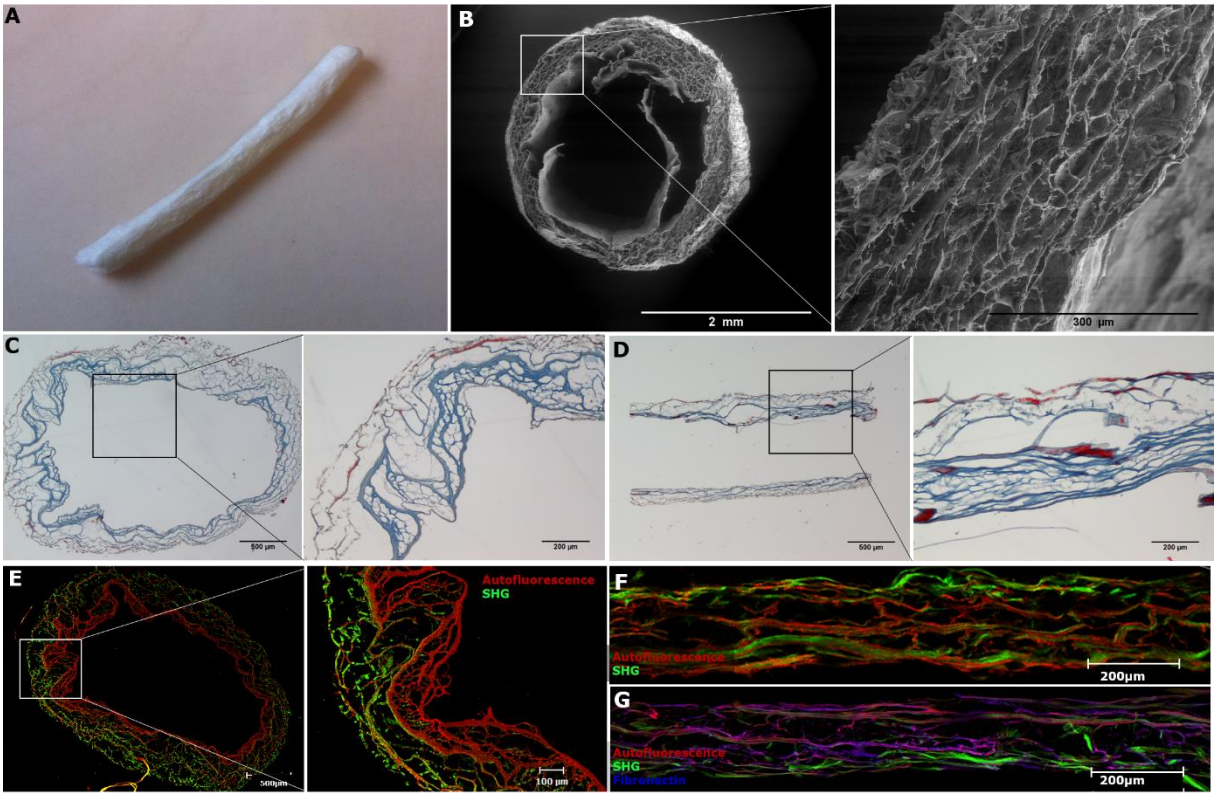


**Figure 14: Intact extracellular matrix (ECM) in decellularized blood vessels. (A)** Macroscopic image of a decellularized blood vessel**. (B)** Scanning electron microscopic images of a decellularized blood vessel with an inner diameter of 2 mm. **(C, D)** A trichrome staining was performed on cross, and longitudal sections of a decellularized blood vessel. No cells were observed in de blood vessel wall, and it seems that the supporting matrix was preserved in the vessel, only the ECM remains. **(E - G)** Label-free optical imaging technique second harmonic generation (SHG) and autofluorescence, with or without fluorescent staining for fibronectin, to characterize the ECM-components of a decellularized blood vessel. As illustrated in (D) collagen type I is located mainly on the outer walls of the vessel (SHG signal in green). The inner vessel shows a lot of autofluorescence which also happens to coincide with the location of fibronectin.

# 4. Discussion

Current therapies for large gap PNIs are autografts and nerve conduits. Both these therapies are insufficient to ensure functional repair. Patients therefore never heal properly from their injury, and must spent the rest of their lives with a partial paralysis. For this reason, much research is focused on finding alternatives that are better able to establish functional repair. These novel therapies must be able to bridge the gap between the two nerve ends, and should be able to stimulate and support the growth of injured axons (5, 7, 8). In this study, the platelet concentrate L-PRF is investigated as a possible alternative therapy for the repair of large gap PNIs. This biomaterial has several advantages, for example it has the potential to induce regenerative processes by releasing growth factors and due to its fibrin matrix, it can provide structural support for regenerating axons (15, 16, 19). We tested this hypothesis in our study by performing several *in vitro* experiments, and testing in an *in vivo* model for PNI.

We aim to use L-PRF for tissue engineering purposes, therefore, it was important to characterize the morphology and 3D fibrin structure in more detail. We demonstrated that L-PRF consists of two definable areas, namely a fibrin-matrix, and a cell-rich area separated by platelet-rich zone. The largest part of the L-PRF clot consists of a dense network of fibrin fibres in which clusters of activated blood platelets are distributed. The cell-rich area is located on one side of the clot, and contains mainly leukocytes (e.g. neutrophils, monocytes) but also some remnants of red blood cells. These leukocytes are surrounded by 'islands' of CD41-positive platelets.

The fibrin fibres in L-PRF play an important role during the recovery of large gap nerve injuries. Fibrin is an ECM component not present in the peripheral nerve in normal healthy conditions, however during PNI fibrin is deposited at the site of injury. Hereby, forming a temporary ECM at the lesion that will aid cell adhesion, and support the growth of regenerating axons (24-26). Furthermore, fibrin has been shown to promote axonal regrowth during nerve regeneration. The use of nerve conduits filled with fibrin hydrogels or made from fibrin glues have shown favourable results in PNI. Nerve conduits with fibrin all aid the nerve regeneration, and the myelination although a nerve autograft still shows better results (24-26). Despite the good results with fibrin nerve conduits, the use of L-PRF for peripheral nerve repair has more advantages. For example, L-PRF is an autologous biomaterial, not from animal origins like fibrin products used in previous studies. The use of L-PRF will therefore have a much lower chance of adverse immune reactions (19-21). Furthermore, the fibrin matrix in L-PRF has a unique 3D-structure that aids the nerve repair. L-PRF is very porous, allowing for axon growth without this growth being blocked by fibrin, while also still giving some structural support to the regenerating axons. This study showed that the ECM component fibronectin, is also present in the fibrin matrix. Fibronectin is found to be co-localized with fibrin. Both fibrin, and fibronectin aid the migration of various leukocytes, and macrophages to the site of injury. Macrophages are needed at the lesion for the initial clearance of the myelin debris (24, 27). Moreover, SC migration is also dependent on the presence of ECM-components (28). However, one study showed that only fibronectin induces SC migration, and that the presence of fibrin might have an adverse effect on the migration. This study suggested that fibrin might act as an antagonist to fibronectin, and thereby hamper the migration of SC to the injury site (29). Furthermore, fibrin induces the SCs to stay in a proliferating, non-myelinating state. Therefore, fibrin clearance is

necessary before nerve regeneration can start properly. (30). In conclusion, all these aspects illustrate the importance of the L-PRF fibrin matrix in peripheral nerve repair.

Previous studies have shown that L-PRF contains many growth factors that originate from blood platelets, and leukocytes. During the production process of L-PRF the blood platelets are activated. These activated blood platelets release their growth factor-rich content, and subsequently many of these growth factors are bound to the fibrin matrix. As a result, these bound growth factors are protected from proteolytic activity, and slowly released from the fibrin matrix over time (15-17, 19, 31). Most growth factors and cytokines stored in α-granules of blood platelets are involved in wound healing, such as connective tissue growth factor (CTGF), epidermal growth factor, IGF-1, platelet factor 4 (PF4), PDGF, transforming growth factor-α (TGF-α), TGF-β1, and VEGF (31, 32). In our study, we characterized the secretome of L-PRF in more detail because we were interested in mediators that have beneficial effects in the context of nerve regeneration. As a first step, we performed an antibody array on L-PRF exudate, and CM. In the protein screening we observed a great variety of different proteins and cytokines present in different donors. For example, the proteins IGF-1, PDGF, TGF-β1, and VEGF were all observed to be present in the exudate, and the CM. The wound healing capacity of these growth factors is reflected in various clinical applications of L-PRF, such as in dental surgeries, and bone regeneration studies (21, 33-36). However, we observed a large variation in expression of these proteins between both the exudate and CM, and between the donors in our study. When comparing different studies that also investigated the growth factors present in L-PRF, we found the same variation between growth factor concentrations (19, 37, 38). Some variation is expected in human blood samples as there is a great genetic diversity between people but several other factors might also influence this variation. Factors like age, gender, and disease might influence the concentration of growth factors present in L-PRF. Additionally, any changes in the fibrin architecture, like compression of the L-PRF clot, may influence the amount of growth factors released, and thus increase the variation present between donors (38, 39).

To analyse the release pattern and concentration of certain growth factors in more detail, we performed an ELISA assay on the L-PRF exudate and CM that was collected at several time points after incubation. We focused on growth factors that are known for their positive effect on nerve regeneration, like the growth factors VEGF, and PDGF which improve the functional recovery after a transection of the sciatic nerve in rats (40, 41). Furthermore, the growth factors NGF, BDNF, GDNF, and NT-3 are all able to stimulate the nerve regeneration (4). In our study, several growth factors, like BDNF, NGF, VEGF, and PDGF, were found to be released slowly over a longer time. The fibrin matrix of L-PRF releases these growth factors for several days. This interesting phenomenon was also confirmed by other studies. These studies have determined that L-PRF still releases growth factors after seven days (19, 37, 38, 42).

As a next step we investigated whether the growth factors released by L-PRF had an effect on the cell survival and neurite growth *in vitro*. We cultured DRG neurons under serum deprived conditions and stimulated them with varying concentrations of exudate and CM. Culturing under serum deprived conditions was done to induce cell stress, and cell death. We observed that the cell survival rate, and more importantly the survival of neurons, was significantly increased when neurons were stimulated with L-PRF CM. Moreover, DRGs showed a significant dose-dependent increase in total neurite length,

neurite length per neuron, number of neurites per neuron and number of branches per neurite when stimulated with CM. Surprisingly, we did not observe these positive effects with the exudate, which implicates that certain factors might be absent in the exudate or that the concentration of certain factors is too low in the exudate to have an effect. Growth factors like BDNF and NGF were present in high amounts in the CM, and only low concentrations were detected in the exudate. It is well-known that these two factors can stimulate axon growth (4). We also found that the percentage of neurons in our culturing conditions compared to all the cells detected was low. This implicates that we have a mixed neuronal cell culture. It is important to define the other cell populations in order to fully understand the effect of L-PRF *in vitro*. Therefore, we performed immuno-double-staining for BIII tubulin, S100 and GFAP (SCs), and fibronectin as a potential 'fibroblast' marker. From these staining we determined that most other cells in our culture are SCs. Therefore, all positive effects observed on the cell survival and neurite growth because of L-PRF, can be either direct effects on the neurons, or indirect effects caused by the stimulation SCs. These findings were confirmed by Zheng *et al.* and Qin *et al.* who demonstrated that PRP and L-PRF can stimulate SC migration, proliferation, and triggers them to secrete neurotrophic factors (43-45). This is also of importance for the *in vivo* situation because of the important role SCs play in the nerve regeneration. When a nerve injury occurs SCs will proliferate, support macrophages in the debris clearance, and form bands of Büngner. Furthermore, SC also secrete various neurotropic factors, like GDNF and NGF, which aid the axon regeneration (2, 4, 6).

As a final step, we performed a pilot experiment to study the effect of L-PRF on nerve repair *in vivo*. Therefore, we chose to use a rat model of sciatic nerve injury as previously described (10, 46). The induction of PNI in sciatic nerves of rats is very well described in many studies. The sciatic nerve is the largest nerve and contains both motor and sensory nerves. Moreover, the nerve is easy to reach, and all functional changes can be directly observed in the affected paw. It is important to note that this model has certain limitations because we cannot mimic large gap nerve defects in rodents when compared to the human situation (47). However, these models are an initial step to test the effect of L-PRF on axon regeneration and functional recovery *in vivo*. In this study, we compared three different treatment groups. The first treatment group was an autograft group, the current 'gold standard' in the clinic. In this group the sciatic nerve was inverted to stimulate the morphometric mismatch that often occurs in the clinic. The morphometric mismatch is one of the reasons why autografts are often insufficient in inducing functional repair (4, 5). The next treatment group was the empty conduit group which was used to bridge the gap between the nerves, and its main purpose was as a control to see if it helped guide the nerve regeneration by giving structural support. The last treatment group was the L-PRF filled conduit group. In this group the conduit was filled with L-PRF to assess the neurogenerative capabilities of L-PRF *in vivo*. L-PRF for *in vivo* implantation needs to be made just before it is used, as older clots will have already lost many growth factors. Furthermore, when placing L-PRF in the conduit, it is crucial that the clot is compressed as little as possible because as mentioned before compression of the clot might result in the loss of many growth factors. In our pilot experiment we followed the rats for two weeks post-surgery to determine the effect of L-PRF on the early nerve repair stages. During these two weeks no toxic or adverse immune reactions against the conduit or L-PRF were observed proving that it is suitable for use in the rat model.

Functional recovery in the rats was assessed with running track analysis via the Catwalk XT. Baseline measurements from before the induction of the nerve injury were compared to measurements made two weeks after surgery. The functional recovery was assessed in the three treatment groups, mentioned earlier. After two weeks, no functional recovery was observed. However, we did see some changes in the RI and phase dispersion limb coordination parameters. All treatment groups showed a worsened coordination after two weeks when compared to the baseline. Furthermore, a decline in the max contact area, stride length, and swing speed was also observed. The decline in these parameters all point to dysfunction of the left hind paw. We also attempted to measure the sciatic function index (SFI) of the rats, however, we observed that in the short recovery period, the rats still did not put down their affected paw when walking. The rats in all treatment groups presented with drop foot and clawed their paws, making it impossible to measure the SFI. This observation is in accordance with findings from Monte-Raso *et al.* who showed that it is very difficult to measure SFI before at least some functional recovery has taken place as the measurements are hampered by the paresis of the affected paw (48). A longer follow-up period after injury should help to better analyse the functional recovery, other studies investigating large gap sciatic nerve injuries (10 mm gap) followed the animals for 30 days (49) or 12 weeks (40, 41) to fully analyse the functional recovery.

After the follow-up period, the cell infiltration into the sciatic nerve lesions of the rats in all three treatment groups was investigated. We did this by immunostaining for SCs (S100), and macrophages (IBA-1) at the proximal ends of the nerves. Cell infiltration is an important first step in the regeneration process (4). Our data showed a lot of infiltration of cells into the three treatment groups, many of these cells were identified to be SCs, and macrophages. It is important to note that it seemed like there was only little SC infiltration into the L-PRF filled conduit group. However, it is likely that this smaller amount of SCs might be coincidental as only one nerve from one rat was stained. Additionally, no quantification of the SC infiltration was done, thus further analysis is needed to make a conclusion on the SC infiltration. Moreover, Qin *et al* has already shown that L-PRF can improve functional nerve recovery in a sciatic nerve injury rat model for crush injury, suggesting that L-PRF can exert a positive influence *in vivo* (43). This study is a favourable sign that L-PRF can also stimulate the nerve regeneration in large gap PNIs *in vivo*.

In this study, we aim to implant L-PRF (the fibrin and platelet-rich area) *in vivo*. However, L-PRF is a very 'elastic' structure and it has no supporting functions, which makes it difficult to implant this biomaterial between two nerve endings *in vivo*. Therefore, we chose to use decellularized blood vessels as conduits to support both L-PRF, and nerve regeneration. The suitability of the conduit was assessed by showing that no foreign antigen (HLA-DR) was left in the vessel which is necessary to avoid adverse immune reactions. Hereafter, we examined the structure of the conduit more closely, and observed that all cells were removed from the vessels. Furthermore, only the ECM of the blood vessels remained, resulting in a conduit that was able to support L-PRF, and the axon regeneration *in vivo*. Additionally, when implanted in the nerve, the conduit showed no adverse effects in any rats, and did not seem to collapse in on itself. Moreover, this decellularized blood vessel meets the important requirements for a good conduit. It is flexible, permeable, and is able to provide some support for the nerve (38, 39).

In the future, L-PRF can be characterized more by determining and quantifying the porosity of the fibrin matrix as we want to use L-PRF for tissue engineering, and as support for axon regeneration. The neurite outgrowth can also be assessed in a 3D-collagen scaffold culture. (50, 51). In the 3D-cultures a whole DRG can be cultured. This ganglion will then still contain many other cells like for example SCs. Therefore, these 3D-cultures can better mimic the *in vivo* situation, this because the other cells in the culture will also influence the neurite outgrowth. Next, a complete *in vivo* study using the rat nerve injury model can be set up in the future. Hereby, utilizing a bigger rat population to exclude any variation that may occur. Furthermore, to fully analyse the functional recovery, the rats need to be followed up for several weeks. Functional analysis of the rats should then be performed at least weekly to assess possible differences between autografts, and L-PRF treated groups. Additionally, it will also be interesting to investigate the morphology of the nerves and their connected muscle at different time points during the study, thereby analysing the nerve regeneration over time. This way histological results can support the *in vivo* functional analysis to get a complete picture of the regeneration. Examples of possible histological analyses are: calculation of the G-ratio of the nerves, quantification of the infiltration of cells (e.g. macrophages and SCs), quantification of the regeneration of the nerves, and quantification of the atrophy in the muscles (52, 53). An example of another future histological assessment, is to examine the phenotypes of SCs in the lesion. During PNI, many SCs revert to an immature phenotype as they lose contact with the axons (54, 55). Furthermore, as previously mentioned, fibrin may halt the SCs in a proliferating, non-myelinating state, and hereby hamper the nerve regeneration. Therefore, assessing the phenotype of the SCs during the recovery process may also give an indication of how they aid the nerve regeneration. Another great future addition to support the *in vivo* functional analysis data is to perform an electrophysiological analysis of the nerves, and their connected muscles This way it can be assessed if the electrical impulses sent through the nerve are able to reach the muscle (56). Additionally, more L-PRF donors should be used in future studies. In the current pilot study only one donor was used, and any results seen can be donor related. More L-PRF donors will exclude any possible donor variability. Lastly, when rat *in vivo* results show improved nerve regeneration, a bigger animal model (e.g. sheep (47)) might be used to repeat the study to better mimic the human situation. A bigger animal model allows us to be able to study a larger nerve gap *in vivo*.

In conclusion, L-PRF is an autologous biomaterial that consists of a fibrin matrix, and a cell-rich area separated by a platelet-rich zone. This fibrin matrix can support and stimulate nerve regeneration. Furthermore, L-PRF slowly releases a plethora of growth factors which are beneficial for the nerve generation, and have been proven to enhance neurite outgrowth *in vitro*. An *in vivo* rat nerve injury model can be used to assess the neuroregenerative capabilities of L-PRF, before a bigger animal model can then be used to better mimic the human situation.

# 5. Conclusion

PNIs represent a major clinical concern worldwide, and current therapies for large gaps PNIs are insufficient to restore lost functions. Therefore, in our study we focus on a new therapeutic approach to augment the nerve regeneration after injury. We speculated that L-PRF, a platelet concentrate consisting of a fibrin network that contains growth factors, platelets, and leukocytes can be used as an alternative therapy. Therefore, we hypothesized that L-PRF promotes functional recovery after PNI by stimulating and supporting the axon regeneration.

From the current study, we can conclude that the fibrin matrix consists of two clearly definable areas. The fibrin matrix containing a lot of activated blood platelets which is separated from the leukocyte filled cell-rich area by a platelet-rich zone. The fibrin matrix of L-PRF can help stimulate and support the nerve regeneration. Furthermore, growth factors, that are able to stimulate nerve regeneration, are trapped in the fibrin matrix, and released continuously over several days. L-PRF can thus serve as a great reservoir of growth factors when implanted *in vivo*. Moreover, the L-PRF growth factors have been proven to stimulate neurite outgrowth and cell survival of DRG neurons *in vitro*. L-PRF shows no toxic effects when implanted in rats. In addition, L-PRF also aids the cell infiltration in the initial phases of nerve regeneration *in vivo*.

In conclusion, the results of this study still fully support L-PRF as a possible alternative therapy for large gap nerve injuries. The advantages of L-PRF are the easy way it is obtained from the peripheral blood, and the low cost of producing this biomaterial is also a positive aspect. Furthermore, L-PRF is an autologous product (produced from patient's own blood) and it will therefore not cause any adverse immune reactions. However, further characterization of this biomaterial both *in vitro* and *in vivo* is necessary to understand its full potential as a therapy for peripheral nerve repair

In the future, we need to quantify the porosity of the fibrin matrix as the intention is to use it for tissue engineering and as support for axon regeneration. Moreover, we should further explore the neuroregenerative potential of L-PRF *in vivo*. A longer follow-up period is needed to investigate the full effect of L-PRF on axon regeneration and functional recovery *in vivo*. Detailed functional testing by comparing several gait parameters, and electrophysiological measurements will aid in the assessment of the functional recovery *in vivo*. Additionally, histological analysis of the regenerated nerves, and affected muscles can support the *in vivo* functional analysis to get a complete picture of the regeneration. Once proven in a rat model, the neuroregenerative capabilities of L-PRF can be shown in a bigger animal model (e.g. sheep) which can better mimic the human situation. These *in vitro* and *in vivo* experiments are necessary to define the true neuroregenerative capabilities of L-PRF.

## References


1. Menorca RM, Fussell TS, Elfar JC. Nerve physiology: mechanisms of injury and recovery. Hand clinics. 2013;29(3):317-30.
2. Arslantunali D, Dursun T, Yucel D, Hasirci N, Hasirci V. Peripheral nerve conduits: technology update. Medical Devices (Auckland, NZ). 2014;7:405-24.
3. Li R, Liu Z, Pan Y, Chen L, Zhang Z, Lu L. Peripheral Nerve Injuries Treatment: a Systematic Review. Cell Biochemistry and Biophysics. 2014;68(3):449-54.
4. Faroni A, Mobasseri SA, Kingham PJ, Reid AJ. Peripheral nerve regeneration: Experimental strategies and future perspectives. Advanced Drug Delivery Reviews. 2015;82-83(Supplement C):160-7.
5. Grinsell D, Keating CP. Peripheral Nerve Reconstruction after Injury: A Review of Clinical and Experimental Therapies. BioMed Research International. 2014;2014:698256.
6. Rui Damásio Alvites ARCS, Artur Severo Proença Varejão and Ana Colette Pereira de Castro Osório Maurício. Olfactory Mucosa Mesenchymal Stem Cells and Biomaterials: A New Combination to Regenerative Therapies after Peripheral Nerve Injury, Mesenchymal Stem Cells - Isolation, Characterization and Applications: InTech; 2017.
7. Pyatin VF, Kolsanov AV, Shirolapov IV. Recent medical techniques for peripheral nerve repair: Clinico-physiological advantages of artificial nerve guidance conduits. Advances in Gerontology. 2017;7(2):148-54.
8. Pabari A, Yang SY, Seifalian AM, Mosahebi A. Modern surgical management of peripheral nerve gap. Journal of Plastic, Reconstructive & Aesthetic Surgery. 2010;63(12):1941-8.
9. Martens W, Sanen K, Georgiou M, Struys T, Bronckaers A, Ameloot M, et al. Human dental pulp stem cells can differentiate into Schwann cells and promote and guide neurite outgrowth in an aligned tissue-engineered collagen construct in vitro. The FASEB Journal. 2014;28(4):1634-43.
10. Sanen K, Martens W, Georgiou M, Ameloot M, Lambrichts I, Phillips J. Engineered neural tissue with Schwann cell differentiated human dental pulp stem cells: potential for peripheral nerve repair? Journal of tissue engineering and regenerative medicine. 2017;11(12):3362-72.
11. Nectow AR, Marra KG, Kaplan DL. Biomaterials for the Development of Peripheral Nerve Guidance Conduits. Tissue Engineering Part B, Reviews. 2012;18(1):40-50.
12. Ruijs AC, Jaquet JB, Kalmijn S, Giele H, Hovius SE. Median and ulnar nerve injuries: a meta-analysis of predictors of motor and sensory recovery after modern microsurgical nerve repair. Plastic and reconstructive surgery. 2005;116(2):484-94; discussion 95-6.
13. Lundborg G. A 25-year perspective of peripheral nerve surgery: Evolving neuroscientific concepts and clinical significance. The Journal of Hand Surgery. 2000;25(3):391-414.
14. Millesi H, Meissl G, Berger A. The interfascicular nerve-grafting of the median and ulnar nerves. The Journal of bone and joint surgery American volume. 1972;54(4):727-50.
15. Bielecki T, Dohan Ehrenfest DM. Platelet-rich plasma (PRP) and Platelet-Rich Fibrin (PRF): surgical adjuvants, preparations for in situ regenerative medicine and tools for tissue engineering. Curr Pharm Biotechnol. 2012;13(7):1121-30.
16. Dohan DM, Choukroun J, Diss A, Dohan SL, Dohan AJJ, Mouhyi J, et al. Platelet-rich fibrin (PRF): A second-generation platelet concentrate. Part I: Technological concepts and evolution. Oral Surgery, Oral Medicine, Oral Pathology and Oral Radiology.101(3):e37-e44.
17. Dohan DM, Choukroun J, Diss A, Dohan SL, Dohan AJJ, Mouhyi J, et al. Platelet-rich fibrin (PRF): A second-generation platelet concentrate. Part II: Platelet-related biologic features. Oral Surgery, Oral Medicine, Oral Pathology and Oral Radiology.101(3):e45-e50.
18. Choukroun J AF, Schoeffler C , Vervelle A. Une opportunité en paro-implantologie: le PRF. Implantodontie. 2000;42:55-62.
19. Schär MO, Diaz-Romero J, Kohl S, Zumstein MA, Nesic D. Platelet-rich Concentrates Differentially Release Growth Factors and Induce Cell Migration In Vitro. Clinical Orthopaedics and Related Research®. 2015;473(5):1635-43.
20. Munoz F, Jiménez C, Espinoza D, Vervelle A, Beugnet J, Haidar Z. Use of leukocyte and platelet-rich fibrin (L-PRF) in periodontally accelerated osteogenic orthodontics (PAOO): Clinical effects on edema and pain. Journal of Clinical and Experimental Dentistry. 2016;8(2):e119-e24.
21. Marenzi G, Riccitiello F, Tia M, di Lauro A, Sammartino G. Influence of Leukocyte- and Platelet-Rich Fibrin (L-PRF) in the Healing of Simple Postextraction Sockets: A Split-Mouth Study. BioMed Research International. 2015;2015:369273.
22. Choukroun J, Diss A, Simonpieri A, Girard M-O, Schoeffler C, Dohan SL, et al. Platelet-rich fibrin (PRF): A second-generation platelet concentrate. Part IV: Clinical effects on tissue healing. Oral Surgery, Oral Medicine, Oral Pathology and Oral Radiology.101(3):e56-e60.

23. Olausson M, Patil PB, Kuna VK, Chougule P, Hernandez N, Methe K, et al. Transplantation of an allogeneic vein bioengineered with autologous stem cells: a proof-of-concept study. Lancet. 2012;380(9838):230-7.
24. Pettersson J, Kalbermatten D, McGrath A, Novikova LN. Biodegradable fibrin conduit promotes long-term regeneration after peripheral nerve injury in adult rats. Journal of Plastic, Reconstructive & Aesthetic Surgery. 2010;63(11):1893-9.
25. Kalbermatten DF, Pettersson J, Kingham PJ, Pierer G, Wiberg M, Terenghi G. New fibrin conduit for peripheral nerve repair. J Reconstr Microsurg. 2009;25(1):27-33.
26. Losso LMV, Carlos MdFJ, Cesar I, Coelho NA, Hopfgartner TN, Rolf G. Comparisons of the results of peripheral nerve defect repair with fibrin conduit and autologous nerve graft: An experimental study in rats. Microsurgery. 2016;36(1):59-65.
27. Digiacomo G, Tusa I, Bacci M, Cipolleschi MG, Dello Sbarba P, Rovida E. Fibronectin induces macrophage migration through a SFK-FAK/CSF-1R pathway. Cell Adhesion & Migration. 2017;11(4):327-37.
28. Liu HM. The role of extracellular matrix in peripheral nerve regeneration: a wound chamber study. Acta neuropathologica. 1992;83(5):469-74.
29. Akassoglou K, Akpinar P, Murray S, Strickland S. Fibrin is a regulator of Schwann cell migration after sciatic nerve injury in mice. Neuroscience Letters. 2003;338(3):185-8.
30. Akassoglou K, Yu W-M, Akpinar P, Strickland S. Fibrin Inhibits Peripheral Nerve Remyelination by Regulating Schwann Cell Differentiation. Neuron. 2002;33(6):861-75.
31. Lundquist R, Dziegiel MH, Agren MS. Bioactivity and stability of endogenous fibrogenic factors in platelet-rich fibrin. Wound repair and regeneration : official publication of the Wound Healing Society [and] the European Tissue Repair Society. 2008;16(3):356-63.
32. Anitua E, Andia I, Ardanza B, Nurden P, Nurden AT. Autologous platelets as a source of proteins for healing and tissue regeneration. Thrombosis and haemostasis. 2004;91(1):4-15.
33. Cano-Durán JA, Peña-Cardelles J-F, Ortega-Concepción D, Paredes-Rodríguez VM, García-Riart M, López-Quiles J. The role of Leucocyte-rich and platelet-rich fibrin (L-PRF) in the treatment of the medication-related osteonecrosis of the jaws (MRONJ). Journal of Clinical and Experimental Dentistry. 2017;9(8):e1051-e9.
34. Castro AB, Meschi N, Temmerman A, Pinto N, Lambrechts P, Teughels W, et al. Regenerative potential of leucocyte- and platelet-rich fibrin. Part B: sinus floor elevation, alveolar ridge preservation and implant therapy. A systematic review. Journal of Clinical Periodontology. 2017;44(2):225-34.
35. Castro AB, Meschi N, Temmerman A, Pinto N, Lambrechts P, Teughels W, et al. Regenerative potential of leucocyte- and platelet-rich fibrin. Part A: intra-bony defects, furcation defects and periodontal plastic surgery. A systematic review and meta-analysis. Journal of Clinical Periodontology. 2017;44(1):67-82.
36. Verma UP, Yadav RK, Dixit M, Gupta A. Platelet-rich Fibrin: A Paradigm in Periodontal Therapy – A Systematic Review. Journal of International Society of Preventive & Community Dentistry. 2017;7(5):227-33.
37. Dohan Ehrenfest DM, de Peppo GM, Doglioli P, Sammartino G. Slow release of growth factors and thrombospondin-1 in Choukroun's platelet-rich fibrin (PRF): a gold standard to achieve for all surgical platelet concentrates technologies. Growth factors (Chur, Switzerland). 2009;27(1):63-9.
38. M. Dohan Ehrenfest D, Bielecki T, Jimbo R, Barbe G, Del Corso M, Inchingolo F, et al. Do the Fibrin Architecture and Leukocyte Content Influence the Growth Factor Release of Platelet Concentrates? An Evidence-based Answer Comparing a Pure Platelet-Rich Plasma (P-PRP) Gel and a Leukocyte- and Platelet-Rich Fibrin (L-PRF). Current Pharmaceutical Biotechnology. 2012;13(7):1145-52.
39. Dohan Ehrenfest DM, Del Corso M, Diss A, Mouhyi J, Charrier JB. Three-dimensional architecture and cell composition of a Choukroun's platelet-rich fibrin clot and membrane. Journal of periodontology. 2010;81(4):546-55.
40. Mohammadi R, Ahsan S, Masoumi M, Amini K. Vascular endothelial growth factor promotes peripheral nerve regeneration after sciatic nerve transection in rat. Chinese journal of traumatology = Zhonghua chuang shang za zhi. 2013;16(6):323-9.
41. Golzadeh A, Mohammadi R. Effect of local administration of platelet-derived growth factor B on functional recovery of peripheral nerve regeneration: A sciatic nerve transection model. Dental Research Journal. 2016;13(3):225-32.
42. Zumstein MA, Berger S, Schober M, Boileau P, Nyffeler RW, Horn M, et al. Leukocyte- and platelet-rich fibrin (L-PRF) for long-term delivery of growth factor in rotator cuff repair: review, preliminary results and future directions. Curr Pharm Biotechnol. 2012;13(7):1196-206.

43. Qin J, Wang L, Sun Y, Sun X, Wen C, Shahmoradi M, et al. Concentrated growth factor increases Schwann cell proliferation and neurotrophic factor secretion and promotes functional nerve recovery in vivo. International journal of molecular medicine. 2016;37(2):493-500.
44. Canbin Z, Qingtang Z, Xiaolin L, Xijun H, Caifeng H, Li J, et al. Effect of platelet-rich plasma (PRP) concentration on proliferation, neurotrophic function and migration of Schwann cells in vitro. Journal of tissue engineering and regenerative medicine. 2016;10(5):428-36.
45. Maniwa S, Iwata A, Hirata H, Ochi M. Effects of neurotrophic factors on chemokinesis of Schwann cells in culture. Scandinavian journal of plastic and reconstructive surgery and hand surgery. 2003;37(1):14-7.
46. Georgiou M, Golding JP, Loughlin AJ, Kingham PJ, Phillips JB. Engineered neural tissue with aligned, differentiated adipose-derived stem cells promotes peripheral nerve regeneration across a critical sized defect in rat sciatic nerve. Biomaterials. 2015;37:242-51.
47. Diogo CC, Camassa JA, Pereira JE, Costa LMD, Filipe V, Couto PA, et al. The use of sheep as a model for studying peripheral nerve regeneration following nerve injury: review of the literature. Neurol Res. 2017;39(10):926-39.
48. Monte-Raso VV, Barbieri CH, Mazzer N, Yamasita AC, Barbieri G. Is the Sciatic Functional Index always reliable and reproducible? Journal of Neuroscience Methods. 2008;170(2):255-61.
49. Martina L, Lucas C, Deise SA, Jefferson BS. Effect of platelet rich plasma and platelet rich fibrin on sciatic nerve regeneration in a rat model. Microsurgery. 2013;33(5):383-90.
50. East E, Golding JP, Phillips JB. A versatile 3D culture model facilitates monitoring of astrocytes undergoing reactive gliosis. Journal of tissue engineering and regenerative medicine. 2009;3(8):634-46.
51. Lv D, Yu S-c, Ping Y-f, Wu H, Zhao X, Zhang H, et al. A three-dimensional collagen scaffold cell culture system for screening anti-glioma therapeutics. Oncotarget. 2016;7(35):56904-14.
52. Lichtenfels M, Colomé L, Sebben AD, Braga-Silva J. Effect of platelet rich plasma and platelet rich fibrin on sciatic nerve regeneration in a rat model. Microsurgery. 2013;33(5):383-90.
53. di Summa PG, Kalbermatten DF, Pralong E, Raffoul W, Kingham PJ, Terenghi G. Long-term in vivo regeneration of peripheral nerves through bioengineered nerve grafts. Neuroscience. 2011;181:278-91.
54. Jessen KR, Mirsky R. The origin and development of glial cells in peripheral nerves. Nature reviews Neuroscience. 2005;6(9):671-82.
55. Mirsky R, Jessen KR, Brennan A, Parkinson D, Dong Z, Meier C, et al. Schwann cells as regulators of nerve development. Journal of physiology, Paris. 2002;96(1-2):17-24.
56. M. W, M. M, T. B, H. S, C. K. Comparative electrophysiological, functional, and histological studies of nerve lesions in rats. Microsurgery. 2005;25(6):508-19.

# Auteursrechtelijke overeenkomst

Ik/wij verlenen het wereldwijde auteursrecht voor de ingediende eindverhandeling:
**Leukocyte- and Platelet Rich Fibrin, an autologous biomaterial to improve regeneration of large gap peripheral nerve injuries**

Richting: **Master of Biomedical Sciences-Clinical Molecular Sciences**
Jaar: **2018**

in alle mogelijke mediaformaten, - bestaande en in de toekomst te ontwikkelen - , aan de Universiteit Hasselt.

Niet tegenstaand deze toekenning van het auteursrecht aan de Universiteit Hasselt behoud ik als auteur het recht om de eindverhandeling, - in zijn geheel of gedeeltelijk -, vrij te reproduceren, (her)publiceren of distribueren zonder de toelating te moeten verkrijgen van de Universiteit Hasselt.

Ik bevestig dat de eindverhandeling mijn origineel werk is, en dat ik het recht heb om de rechten te verlenen die in deze overeenkomst worden beschreven. Ik verklaar tevens dat de eindverhandeling, naar mijn weten, het auteursrecht van anderen niet overtreedt.

Ik verklaar tevens dat ik voor het materiaal in de eindverhandeling dat beschermd wordt door het auteursrecht, de nodige toelatingen heb verkregen zodat ik deze ook aan de Universiteit Hasselt kan overdragen en dat dit duidelijk in de tekst en inhoud van de eindverhandeling werd genotificeerd.

Universiteit Hasselt zal mij als auteur(s) van de eindverhandeling identificeren en zal geen wijzigingen aanbrengen aan de eindverhandeling, uitgezonderd deze toegelaten door deze overeenkomst.

Voor akkoord,

**Coekaerts, Lien**

Datum: **7/06/2018**